2-5-2013

Toward Designed Singlet Fission: Solution Photophysics of Two Indirectly Coupled Covalent Dimers of 1,3-Diphenylisobenzofuran

Justin C. Johnson

Akin Akdag

Matibur Zamadar
Stephen F Austin State University, zamadarmr@sfasu.edu

Xudong Chen

Andrew F. Schwerin

See next page for additional authors

THE JOURNAL OF PHYSICAL CHEMISTRY B

Article

pubs.acs.org/JPCB

Toward Designed Singlet Fission: Solution Photophysics of Two Indirectly Coupled Covalent Dimers of 1,3-Diphenylisobenzofuran

Justin C. Johnson,[†] Akin Akdag,[‡,§] Matibur Zamadar,[∥] Xudong Chen,[‡] Andrew F. Schwerin,[‡] Irina Paci,[#] Millicent B. Smith,[‡] Zdeněk Havlas,[⊥] John R. Miller,[∥] Mark A. Ratner,[#] Arthur J. Nozik,[†] and Josef Michl*[,‡,⊥]

[†]National Renewable Energy Laboratory, Golden, Colorado 80401, United States

[‡]Department of Chemistry and Biochemistry, University of Colorado at Boulder, Boulder, Colorado 80309, United States

[§]Department of Chemistry, Middle East Technical University, 06800 Ankara, Turkey

[∥]Chemistry Department, Brookhaven National Laboratory, Building 555A, Upton, New York 11973, United States

[⊥]Institute of Organic Chemistry and Biochemistry, Academy of Sciences of the Czech Republic, 16610 Prague, Czech Republic

[#]Department of Chemistry and Materials Research Center, Northwestern University, Evanston, Illinois 60208, United States

Supporting Information

ABSTRACT: In order to identify optimal conditions for singlet fission, we are examining the photophysics of 1,3-diphenylisobenzofuran (**1**) dimers covalently coupled in various ways. In the two dimers studied presently, the coupling is weak. The subunits are linked via the para position of one of the phenyl substituents, in one case (**2**) through a CH_2 linker and in the other (**3**) directly, but with methyl substituents in ortho positions forcing a nearly perpendicular twist between the two joint phenyl rings. The measurements are accompanied with density functional theory (DFT) and time-dependent DFT (TD-DFT) calculations. Although in neat solid state, **1** undergoes singlet fission with a rate constant higher than 10^{11} s^{-1}; in nonpolar solutions of **2** and **3**, the triplet formation rate constant is less than 10^6 s^{-1} and fluorescence is the only significant event following electronic excitation. In polar solvents, fluorescence is weaker because the initial excited singlet state S_1 equilibrates by sub-nanosecond charge transfer with a nonemissive dipolar species in which a radical cation of **1** is attached to a radical anion of **1**. Most of this charge transfer species decays to S_0, and some is converted into triplet T_1 with a rate constant near 10^8 s^{-1}. Experimental uncertainties prevent an accurate determination of the number of T_1 excitations that result when a single S_1 excitation changes into triplet excitation. It would be one if the charge-transfer species undergoes ordinary intersystem crossing and two if it undergoes the second step of two-step singlet fission. The triplet yield maximizes below room temperature to a value of roughly 9% for **3** and 4% for **2**. Above ~360 K, some of the S_1 molecules of **3** are converted into an isomeric charge-transfer species with a shorter lifetime, possibly with a twisted intramolecular charge transfer (TICT) structure. This is not observed in **2**.

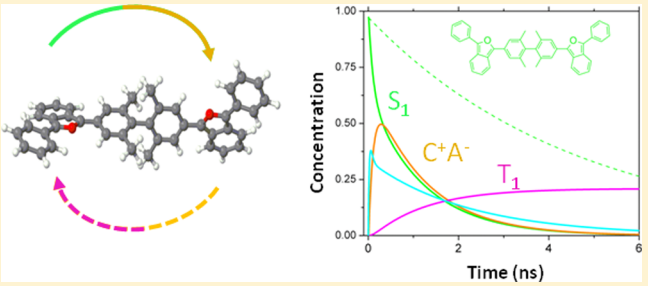

INTRODUCTION

The use of singlet fission[1] represents a promising avenue for improving the efficiency of solar cells.[2] In this process, an excited singlet state of a chromophore shares its energy with a ground state neighbor, producing a triplet excited state of each. If both triplet excitations behaved independently and could be used for free charge carrier generation in a device utilizing both conventional and singlet fission chromophores, the maximum theoretical efficiency would reach ~46%[3] instead of the usual Shockley–Queisser limit of 32%[4] for a single-junction cell.

For practical applications, it would be very useful to have a wide selection of efficient systems. As discussed in more detail elsewhere,[1,5,6] for this purpose it is desirable to optimize (i) the choice of the monomeric chromophore, and (ii) the efficiency of interchromophore coupling, before addressing other concerns, such as redox potentials, independent charge separation from the two triplets, and so on.

Choice of Chromophore. Although singlet fission was observed on a number of crystalline and polymeric chromophores,[1] the measured triplet quantum yields were mostly very small and of little practical interest. Although it has been clear for some time that the longer polyacenes and some carotenes produce triplets efficiently, only recently have triplet yield measurements been made and values well in excess of 100% and mostly near the theoretical limit of 200% were

Special Issue: Paul F. Barbara Memorial Issue

Received: November 6, 2012
Revised: January 31, 2013
Published: February 5, 2013

   dx.doi.org/10.1021/jp310979q | J. Phys. Chem. B 2013, 117, 4680–4695

actually found for solid tetracene,[7] pentacene,[8,9] and a handful of their simply substituted derivatives,[10−13] as well as for aggregated zeaxanthin,[14] a carotenoid. Another solid for which a 200% triplet yield was found is 1,3-diphenylisobenzofuran (**1**).[15]

In the first two full papers of this series,[5,16] we argued that in order to make singlet fission itself slightly exothermic and to make all important modes of T_1-T_1 annihilation endothermic, one should choose chromophores for which not only the energy of the relaxed S_1 and T_1 states, but also that of the T_2 state are appropriate and meet the conditions $E(S_1)$, $E(T_2) \geq 2E(T_1)$. A high yield of fluorescence was identified as another desirable property for the isolated chromophore, since it indicates the absence of competing decay mechanisms such as photochemical transformations or intersystem crossing. Several likely candidates were identified by theoretical means,[5] and 1,3-diphenylisobenzofuran (**1**) was selected as a suitable model for an initial investigation. Its low-lying singlet, triplet, and ionized states were characterized thoroughly,[16] and satisfy the desired criteria. In a solid film at 77 K, **1** was found to produce a 200% yield of triplets. This compound is the first molecule specifically designed for efficiency in singlet fission.

In the present paper we examine two covalent dimers of **1**, coupled only very weakly in order to preserve the identity of their two chromophores. Covalent dimers can be synthesized with a high degree of precise and systematic control of interchromophore coupling, difficult to achieve in crystals of monomers. They are of interest both for fundamental studies of coupling optimization and for potential practical implementations in which they could be adsorbed as individual units on semiconductor support.

Choice of Interchromophore Coupling. Little is known about the degree of interchromophore coupling needed to make singlet fission competitive with fluorescence and yet allow the two triplets, born coupled to an overall singlet, to behave as independent excitations, each capable of free charge carrier generation. It is not even known whether in a covalent dimer these two requirements are not contradictory. Data for covalently linked tetracene pairs[17,18] and initial results for covalently linked pairs of **1**[19] indicate a triplet yield of only a few percent, although in neat solid tetracene and **1**, the yield is close to 200%. The origin of this difference is not clear. It is possible that the crystal environment provides a more favorable interchromophore coupling, by positioning the molecules favorably and/or by stabilizing low-energy charge-transfer states that can serve as virtual states in the coupling process. The inability of the two triplets in the dimer to diffuse apart may be significant as well. It is also possible that the delocalization of the initial excited singlet state in the crystal is helpful in itself, even though the matrix elements between the singlet coupled triplet pair and either the localized or the delocalized initial singlet wave function are known[1] to be nearly the same. Singlet excitation is often delocalized in crystals and aggregates (e.g., J-aggregates[20]), whereas in covalent dimers and oligomers, excitation localization appears to be the rule, albeit with very small energy barriers for moving from one to the other excited minimum (e.g., in triptycene, ∼0.15 kcal/mol[21]), and with exceptions (e.g., excimers).

The interchromophore interaction can range from mere physical contact through indirect covalent coupling via interposed structures to direct covalent bonding that permits strong π-electron conjugation. Strong coupling may not only affect the rate of singlet fission directly, by modulating the coupling matrix elements, but also indirectly, by modifying the energies of the states of the isolated monomers and thus the exoergicity of the singlet fission process. The effect of coupling on the final energy levels in the dimer is thus capable of ruining the validity of the initially designed relations $E(S_1)$, $E(T_2) \geq 2E(T_1)$.

The third full paper in this series[22] used simple molecular orbital (MO) theory to examine the effect of structure on the strength of interchromophore coupling in a series of dimers of three chromophores that are possible candidates for singlet fission studies, and ordered them from weakly to strongly coupled. The coupling strength was estimated very roughly from the splitting of frontier orbital and low-lying state energies when the two chromophores were combined. A more direct procedure would be to evaluate the action of the total electrostatic Hamiltonian on the initial state.[1] Because of the complicated spin dynamics that may occur in singlet fission, the ultimate triplet yield in a dimer could depend on other aspects of its structure as well, such as the relation of the spin−spin dipolar tensors of the two halves, and the splitting of the $^1(TT)$ singlet, $^3(TT)$ triplet, and $^5(TT)$ quintet levels that result from the interaction of two local triplets.

Presently, we have selected linear chromophore coupling, one of the modes that have received theoretical attention, and examine the dimers **2** and **3**.

Singlet Fission Mechanisms. There are at least two ways in which singlet fission mechanism can be classified, and in both, simple limiting cases can be envisaged.

(A) Coherent versus incoherent process. (i) If the chromophores are coupled strongly enough and $E(S_1)$ approximately equals $2E(T_1)$, the process could occur coherently on a femtosecond time scale and be faster than vibrational relaxation, as appears to be the case in solid pentacene.[23] Some theoretical aspects of this possibility have been examined.[24,25] (ii) If the coupling of the chromophores is weak and/or $E(S_1)$ lies too far below $2E(T_1)$, vibrational relaxation will occur first, and singlet fission will be relatively slow (ps time scale), as appears to be the case in polycrystalline **1**.[15] It will then be best understood in terms of motion on the potential energy hypersurfaces that are encountered on the way from the geometry of the initial vertically excited singlet state to that of the final double-triplet excited singlet state, with their minima, barriers, and conical intersections.

(B) Direct versus mediated process.[1] This mechanistic distinction is less well defined in that it depends on the degree of sophistication chosen for the description of the initial and final states. The least elaborate choice is to describe all states in terms of configurations based on orbitals localized on one or the other partner and assumed to be orthogonal. Then, (i) in the first approximation, one describes the initial and final states of the process in terms of excitations strictly localized on a single partner, and the matrix element between them is due to the two-electron part of the total Hamiltonian (the direct contribution to the singlet fission process). (ii) In a better approximation, one allows the initial and final states to contain small admixtures of charge-transfer configurations before evaluating the coupling matrix element between them. This introduces additional terms that result in an indirect coupling of the initial and final strictly locally excited states through the intermediacy of virtual intermediate states of charge-transfer nature. In these terms, the one-electron part of the Hamiltonian plays a dominant role (the mediated contribution to singlet fission). In one imaginable limit, the direct contribution would

dx.doi.org/10.1021/jp310979q | J. Phys. Chem. B 2013, 117, 4680−4695

dominate, and in the other, the mediated contribution would prevail. The relative importance of the mediated contribution is a function not only of the magnitude of the off-diagonal elements in the Hamiltonian matrix written in the strictly localized basis, but also of the differences between diagonal elements (the energies of the charge-transfer states relative to the initial and final states). We have already pointed out above that environmental stabilization of charge-transfer states may be the primary factor that makes singlet fission more efficient in solids than in dimers. In an extreme case, one can imagine that in a highly polar solvent or in a highly polarizable crystal, some of the charge-transfer states are stabilized so much that they become the lowest singlet state somewhere along the reaction coordinate and then represent real rather than virtual intermediates. The singlet fission process would then occur not in a single kinetic step, but in two steps, via an observable charge-transfer intermediate.

The Present Study. We describe the results of our investigation of the first two of the about 10 covalent dimers of the model chromophore **1** that we have synthesized (**2** and **3**, Chart 1, blue = **1**, red = **2**, green = **3**; this color coding is used throughout). In these two dimers, the coupling of the two halves is weak, and we find negligible triplet yields in nonpolar environments. As described below, they rise up to almost 10% at low temperature in highly polar environments where a real charge-transfer intermediate state is observed. These may be the first observations of the stepwise singlet fission discussed just above, but the errors in our quantum yields unfortunately are on the order of a few percent and they do not allow us to distinguish whether the step that leads from a charge-transfer excited molecule to the final product yields one (ordinary intersystem crossing) or two (singlet fission) triplet excitations in the dimer.

Chart 1. Structures 1−3 and Their Ground State Conformers 2syn, 2anti, and 3

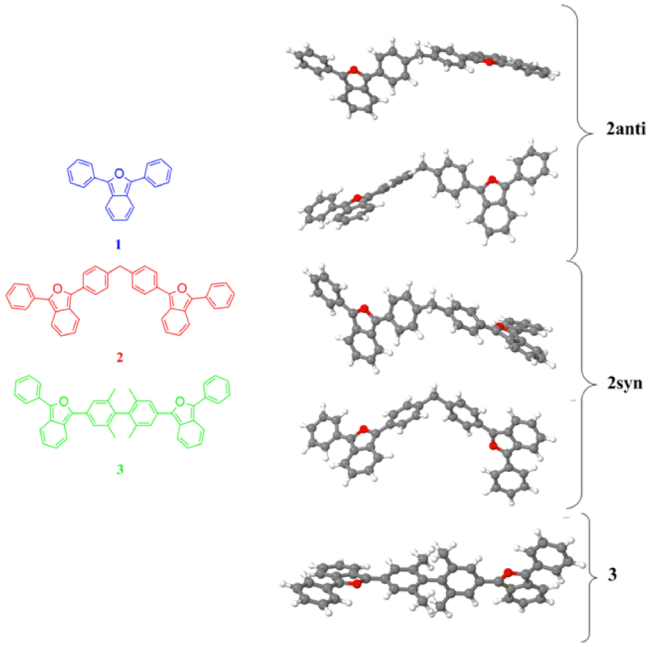

EXPERIMENTAL SECTION

Synthetic Procedures. The syntheses and purification of the covalent dimers **2** and **3** are described in the Supporting Information.

Measurements. Solvents (dimethyl sulfoxide, DMSO; acetonitrile, AN; tetrahydrofuran, THF; cyclohexane, CH; toluene, TOL; *N*,*N*-dimethylformamide, DMF) were purchased from Aldrich (highest purity) and were used as received. They were flushed with argon for at least 30 min before transfer to a glovebox. Sample cells were sealed in the glovebox before being taken into ambient conditions for use. Since **1** is photolabile in the presence of oxygen,[26] **2** and **3** were expected to exhibit a similar instability. The procedures used for measurements resulted in only minor degradation of solutions over the course of hours under continuous (20 mW/cm^2) or pulsed (1 mJ/cm^2, 5 ns pulse) radiation. Significant degradation was observed in minutes under more intense pulsed irradiation, and such conditions were avoided.

Spectroscopic and photophysical measurements were performed as described previously,[16] except that for probe wavelengths below 450 nm, a frequency-doubled beam (pulse width below 50 fs) provided by a noncollinear optical parametric amplifier (NOPA)[27] was used. The procedures followed in the determination of the absorption spectra of the radical cation and radical anion of **3** by pulse radiolysis were the same as in previous work with **1**.[16]

Triplet Yields. Measurements of triplet yields depended on the use of anthracene as sensitizer, and are described in detail in the Supporting Information.

Modeling of Spectrotemporal Data. Global target analysis was performed for **2** and **3** in DMSO and CH, and the details are given in the Supporting Information. The three-dimensional data sets (time delay, wavelength, change in optical density) were used as input into the global analysis program after correcting for the chirp of the probe beam. We used the built-in global analysis in the software package Igor,[28] with a custom fit function. The fit was performed using compartmental analysis in matrix form in order to extract true rate constants for the processes.[29]

Calculations. The procedures are described in detail in the Supporting Information. All calculations were of the density functional theory (DFT) type, and their interpretation needs to take into account the presence of artifacts due to underestimation of the energies of charge-transfer excitations.

RESULTS

Synthesis of 2 and 3. The preparation of the dimers **2** and **3** was analogous to the literature procedure for the preparation of **1** by reaction of phenylmagnesium bromide with 3-phenylphthalide (**4**).[30,31] Use of the double Grignard reagents obtained from bis(*p*-bromophenyl)methane[32] and 4,4′-dibromo-2,2′,6,6′-tetramethylbiphenyl[33] yielded **2** and **3** in 91% yield for both compounds (Scheme 1). Alternatively, the dibromo compounds can be converted to organolithium compounds and treated with **4**.[34] Although the syntheses were facile, the purification was not. The main difficulty was the air sensitivity of these compounds in light. The purification was carried out under argon atmosphere by recrystallization until no traces of impurities were detectable by NMR. The products were stored in the dark under inert atmosphere.

Calculated Geometries of 1−3 (Charts 1 and S1, Table S1 in Supporting Information). *The Ground State.*

dx.doi.org/10.1021/jp310979q | J. Phys. Chem. B 2013, 117, 4680−4695

Scheme 1. Synthetic Routes to 2 and 3

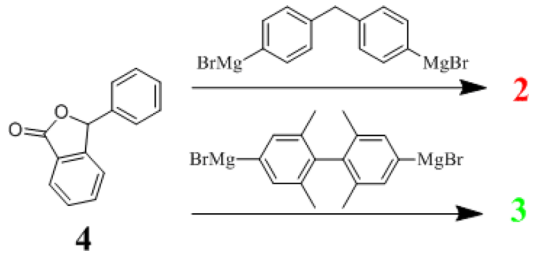

Monomer. The ground-state geometry of one of the two conformers of **1** (C_2 symmetry) is known from single crystal X-ray diffraction, and the bond lengths and angles are in very good agreement with ab initio and density functional theory calculations.[16] The other conformer (C_s) is predicted to have nearly identical bond lengths and angles, but conrotatory rather than disrotatory relative angles of ~18° twist between the planes of the central isobenzofuran moiety and the two phenyl substituents. All calculated properties of the two conformers are very similar, and it was actually difficult to prove their independent existence experimentally. Different shapes of the Franck–Condon envelopes of the first transition are the main differentiating feature.[16]

In the S_1 and T_1 excited states of **1**, the calculated twist angle is only about 5 and 0°, respectively. The molecule is essentially planar and, effectively, only one conformer exists. The strong bond length alternation in the ground state, characteristic of its *o*-quinoid structure, is reduced in the S_1 state, and even more so in the T_1 state.[16]

Dimers. Experimental structural information is not available for **2** and **3**, but their formulas suggest that their ground state bond lengths and angles will be very similar to those of the conformers of **1**, since only a weak interaction can be expected between the two halves. The number of conformers will however be larger, since the two aromatic substituents at positions 1 and 3 of each isobenzofuran are inequivalent and each can be attached with a positive or negative helical sense. We assume that all other ground-state properties of the various conformers of **2** and **3** are also very similar and that it is adequate to calculate the properties of one that is representative. This expectation has been confirmed by calculations for a few conformers, and we have arbitrarily chosen one of the C_2 symmetry minima in the ground state potential energy surface for further work. Chart 2 indicates the labels used to refer to the various angles and bonds in **1**–**3**. Their values optimized in various electronic states are given in Table S1 (Supporting Information).

In addition to the presumably inconsequential conformational isomerism associated with mild twisting of the rings attached to the furan moieties, we need to consider the possibly more important isomerism due to different possible angles of rotation of the two approximately planar π-electron systems **1** around the central bonds in **2** or bond in **3** (see Chart 2). Two major conformers of **2** were subjected to geometry optimization. The **2anti** conformer is more stable by 0.47 kcal/mol. It has C_2 symmetry, ω_3 is −89.3°, and the isobenzofuran moieties are oriented anti to each other. Rotation of one of the monomers until ω_3 reached nearly 0°, followed by geometry optimization, converted the **2anti** to the **2syn** conformer, in which the mutual disposition of the isobenzofuran moieties is syn.

Geometry optimization of **3** revealed an almost exactly orthogonal twist around the central C–C bond. The two enantiomers of this chiral C_2 structure **3** are interconverted by a 180° internal rotation about the central C–C bond. The geometry of each half of the molecule is nearly equal to that of **1**, except that the phenyl twist angles deviate slightly.

The C_2 symmetric ground state geometries of **1**, **2anti**, and **3** were used as initial points for the optimization of the first singlet, triplet, and quintet excited state geometries.

The First Excited Singlet State (S_1). In **2** and **3**, the calculations clearly localize the excitation in one of the chromophores, whose geometry is nearly planar (in **2**, ω_1 = 5 ° and ω_2 = 2 °) and very close to that of the S_1 geometry of **1**, whereas the other is somewhat twisted (in **2**, ω_4 = 15 ° and ω_5 = 12 °) and close to the S_0 geometry of **1**. In agreement with these observations, the adiabatic S_0–S_1 excitation energies calculated for **2** and **3** (58.1 and 59.2 kcal/mol, respectively) are only a little different from that calculated for **1** (61.8 kcal/mol). The solvent effect on the energy of the S_1 state is computed (COSMO, DMSO, ε = 46.7) to be similar to that in **1** (Table 1).

The First Triplet State (T_1). In the dimers **2** and **3**, triplet excitation is also calculated to be localized on one of the chromophores, whose geometry resembles that of the T_1 state of **1**, while the geometry of the other is very close to that of the S_0 state of **1**. In agreement with this observation, the adiabatic S_0–T_1 excitation energies for **1**–**3** are calculated to be nearly identical (33.2, 32.9, and 33.0 kcal/mol, respectively). The triplet excitation energies are not affected by inclusion of COSMO solvation (DMSO, ε = 46.7) in the calculation (Table 1).

Chart 2. Definition of Geometrical Parameters in 1–3

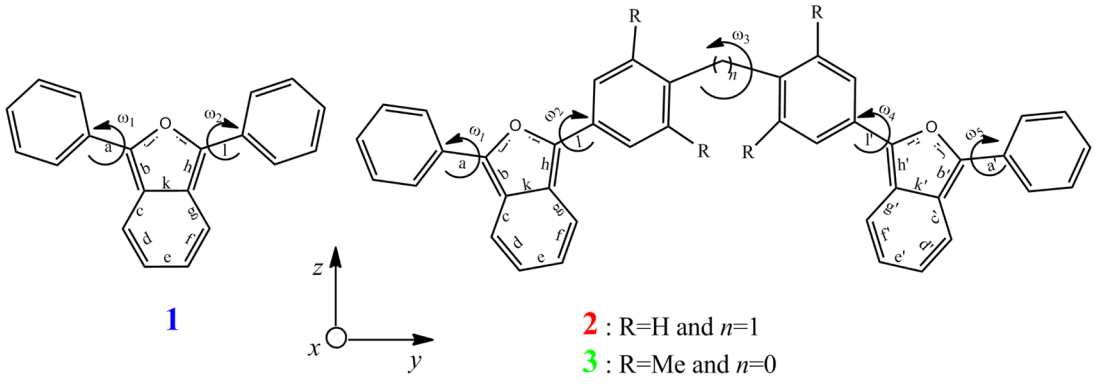

dx.doi.org/10.1021/jp310979q | J. Phys. Chem. B 2013, 117, 4680–4695

Table 1. Optimized States of 1−3: DFT Energies (B3LYP/SVP without and with COSMO, DMSO, ε = 46.7) Relative to the Ground State; in Square Brackets, the Solvent Stabilization Energy (kcal/mol)[a,b]

species	state	gas phase[a]	DMSO solution[a]
1	S_0	0	0 [−6.1]
	S_1	61.8	54.7 [−13.2]
	T_1	33.2	32.9 [−6.4]
2	S_0	0	0 [−12.1]
	S_1	58.1	54.3 [−16.2]
	T_1	32.9	32.7 [−12.3]
	^{1}(TT)	66.0[b]	65.3[b] [−12.8]
	^{5}(TT) = Q_1	65.9[b]	65.6[b] [−12.4]
	(CA)[c]	96.1[b]	65.7[b]
	C	136.1	111.2 [−36.9]
	A	−26.3	−54.7 [−40.5]
	C and A[d]	109.8	56.5 [−77.4]
3	S_0	0	0 [−11.6]
	S_1	59.2	54.2 [−16.6]
	T_1	33.0	32.8 [−11.8]
	^{1}(TT)	66.1[b]	65.5[b] [−12.2]
	^{5}(TT) = Q_1	66.0[b]	65.6[b] [−12.0]
	(CA)[c]	85.7[b]	61.1[b]
	C	136.0	111.2 [−36.4]
	A	−25.6	−54.3 [−40.3]
	C and A[d]	110.4	56.9 [−76.7]

[a]Calculated using the Gaussian program. [b]Calculated using the NWChem program. [c]Intramolecular charge-transfer state, C stands for radical cation and A for radical anion; constrained DFT. [d]IP, separated ion pair.

Double Triplet States: Quintet ^{5}(TT) and Singlet ^{1}(TT). The computer programs available to us permitted calculations for the quintet ^{5}(TT) and singlet ^{1}(TT) levels that result from the coupling of two T_1 states, one on each half of the covalent dimer, but not for the triplet ^{3}(TT). Since the results for ^{5}(TT) and ^{1}(TT) were nearly identical (Table 1), it is safe to assume that they would be no different for ^{3}(TT).

The optimized geometries of the double triplet states of the dimers **2** and **3** have C_2 symmetry. In each half, the geometry is essentially indistinguishable from that of triplet **1**. The central dihedral angle ω_3 is similar to that in the S_0 state. In line with the description of the quintet state as carrying a triplet excitation on each of the two chromophores **1**, the computed adiabatic S_0−Q_1 excitation energies of **2** and **3** are 65.9 and 66.0 kcal/mol, respectively, essentially exactly twice their triplet excitation energy, and only 0.4 kcal/mol less than twice the triplet excitation energy of the monomer **1**. Explicit consideration of the DMSO solvent has little effect (Table 1).

The Intramolecular Charge-Transfer State (CT). The CDFT/B3LYP/SVP gas-phase optimized geometries of the charge-transfer states of **2** and **3** (Chart S1 and Table S1) consist of radical cation and radical anion halves that are very close to the published[16] calculated geometries of the monomeric radical cation and radical anion of **1**, respectively. In **2**, the 104° valence angle between the chromophores at the central methylene group is much smaller than the 115° computed for the ground state. In **3**, the calculated dihedral angle between the mean planes of the two halves is 78°, significantly lower than the 90° calculated for the ground state. The very high CDFT B3LYP/SVP gas phase energy of the charge-transfer states of **2** and **3** is reduced by 25−30 kcal/mol upon inclusion of the DMSO solvent (COSMO, ε = 46.7) in the calculation (Table 1), and they become competitive with the double triplet state.

The charge distribution is almost the same when calculated in the absence or presence of the solvent. It is symmetric in that the absolute total charges on the terminal phenyl groups are similar, but both the positive and the negative charges are polarized toward the center of the molecules in comparison with their distribution in the radical cation and radical anion of **1** (Figure S1).

In the discussion of the geometry of the dipolar CT states, we assumed that the separation of the dimer molecules into the cationic and anionic halves occurs symmetrically, by a twist at the center of the dimer. A justification for this is provided by the nearly perfect agreement of the absorption spectra of the CT states of both **2** and **3** with the sum of the spectra of the radical cation and the radical anion of **1**, discussed below. The agreement with the time-dependent DFT (TD-DFT) calculated sum of the spectra is less satisfactory but acceptable. There are problems with this comparison in that each of the two radical ion spectra is taken in a different solvent, and moreover, it is already known[16] that the transition energies of both radical ions of **1** calculated at this level of approximation are too high relative to those observed.

The Twisted Intramolecular Charge-Transfer (TICT) State. Twisting around other single bonds in the dimers could occur as well. Derivatives of monomeric **1** in which one of the phenyl substituents carries electron-withdrawing substituents are known to form TICT states upon excitation in polar solvents.[35] In the TICT state, the plane of the modified phenyl substituent of **1** is believed to be approximately orthogonal to the furan ring, based both on calculations and in analogy to the TICT states of other molecules of the donor−acceptor type,[36] in at least one of which transient orthogonal twisting was proven directly.[37]

Therefore, it appeared possible that at least in **3**, in which the internal phenyl substituents on the isobenzofuran moieties are modified considerably, a similar TICT species, isomeric with the symmetrically twisted CT species described above, might exist. Unfortunately, a CDFT/B3LYP/SVP (COSMO, ε = 46.7) geometry optimization in which either a positive or a negative charge was constrained to the 1-phenylisobenzofuran fragment and an opposite charge was constrained to the 1-(2,6,2′,6′-tetramethylbiphenyl-4-yl)-3-phenylisobenzofuran fragment did not produce satisfactory results. More than one minimum was found, but none had a near orthogonal twist angle at the charge separation point in the dimer. Since this is a side issue in our project, we did not pursue the search further.

The Intermolecular Charge-Transfer State: An Ion Pair (IP). Electron transfer from one molecule of a dimer **2** or **3** to another will generate a radical cation $\mathbf{2}^{+\bullet}$ or $\mathbf{3}^{+\bullet}$ and a radical anion $\mathbf{2}^{-\bullet}$ or $\mathbf{3}^{-\bullet}$ of the dimer. The optimized geometries of these ions (Table S1) and the charge distribution reveal that the radical ion character is localized in one-half of the molecule while the other half is analogous to the ground state of **1**. Since the conditions for solvation of the separated ion pair are optimal, its stabilization by the DMSO solvent is huge (Table 1), and its energy is computed to be significantly below that of the intramolecular charge transfer state.

Calculated Electronic Transitions in 1−3. B3LYP/SVP vertical excitation energies, oscillator strengths if spin-allowed, and polarization directions for low-energy S_0−S_n (Table S2, Figure 1, parts A, B, and D), S_0−T_n (Table S3), and T_1−T_n

dx.doi.org/10.1021/jp310979q | J. Phys. Chem. B 2013, 117, 4680−4695

(Table S4, Figure 2) transitions were calculated at the optimized geometries (Table S1) of the initial states, using the C_2 symmetric conformers of **1**, **2anti**, and **3**. Computational results have also been incorporated in many of the other figures (Figures 3−11). Specifically, Figure 11C shows the calculated spectra of the radical ions of the molecular fragments present in the TICT structure of **3** (Tables S5 and S6 give data for both choices of polarity). Figures 7 and 11B display the calculated absorption spectra of the radical anions and radical cations of **2** and **3** (Table S7). Their sum represents the calculated absorption of the separated ion pair state IP, and can be used to approximate the absorption spectra of the intramolecular CT states of these dimers (Figure 7).

Because of the known inadequacy of the TD-DFT procedure employed here,[38−40] artificial low-energy charge-transfer states are calculated in weakly coupled dimers, and the very weak computed transitions into these states need to be ignored. For instance, four instead of two nearly degenerate low-energy states of the dimer result from the S_0 to S_1 excitation in the monomer. The two that are of locally excited nature are represented correctly, but the two that are of charge-transfer nature are artifacts. Since they have almost no intensity, their presence has virtually no effect on the predicted absorption spectra. In reality, such states occur at much higher energies, as can be seen in Table 1.

The present results for **1** are very similar to those found earlier at a higher level of calculation,[16] and all spectral interpretations remain unchanged. In particular, the S_1 and T_1 states correspond to highest occupied molecular orbital to lowest unoccupied molecular orbital (HOMO−LUMO) promotions.

Absorption from S_0 and Steady-State Emission from S_1. The S_0−S_n absorption and S_1−S_0 fluorescence spectra of **1**−**3** in DMSO are displayed color coded in Figure 1C, and the spectral characteristics measured in four solvents are listed in Table 2. The peak absorption coefficient of **1** in DMSO[16] is 2.5 × 10^3 M^{-1} cm^{-1}, and those of the dimers **2** and **3** are about twice higher, 5.7 × 10^3 and 4.8 × 10^3 M^{-1} cm^{-1}, respectively. The broad lowest absorption band of **2** and **3** peaks near 23 × 10^3 cm^{-1}, only very little below that of **1**. The relative strength of vibronic features changes systematically from **1** to **3**. Adjusting solvent polarity causes a solvatochromic shift of the absorbance maximum for **1**−**3** of less than 250 cm^{-1}, nearly the same in each compound. The first absorption band and the fluorescence of **1**−**3** can be fitted to three Gaussian bands. The relative amplitude of the 0−0 vibronic band is largest in nonpolar solvents and is larger in **2** and **3** than in **1**. Two higher energy absorption bands are observable in the ultraviolet for each compound, near 31 × 10^3 and 38.5 × 10^3 cm^{-1}.

In nonpolar or weakly polar solvents, the fluorescence quantum yield Φ_F of **1**−**3** lies between 0.92 and 1.0. In contrast to **1**, as the solvent polarity is increased, **2** and **3** exhibit a large decrease in Φ_F. However, the shape of the fluorescence spectrum does not change substantially.

Long-Lived Transients. Absorption from T_1. No phosphorescence was observed, even at liquid nitrogen temperature, and the triplet excitation energies are unknown. For **2** and **3**, the same transient T_1−T_n spectra were obtained by anthracene sensitization and upon direct excitation in polar solvent (Figure 2). No T−T absorption is observed upon direct excitation in nonpolar solvents. The spectra were measured both by steady-state photomodulation and by flash photolysis. The directly excited spectra were used to evaluate triplet

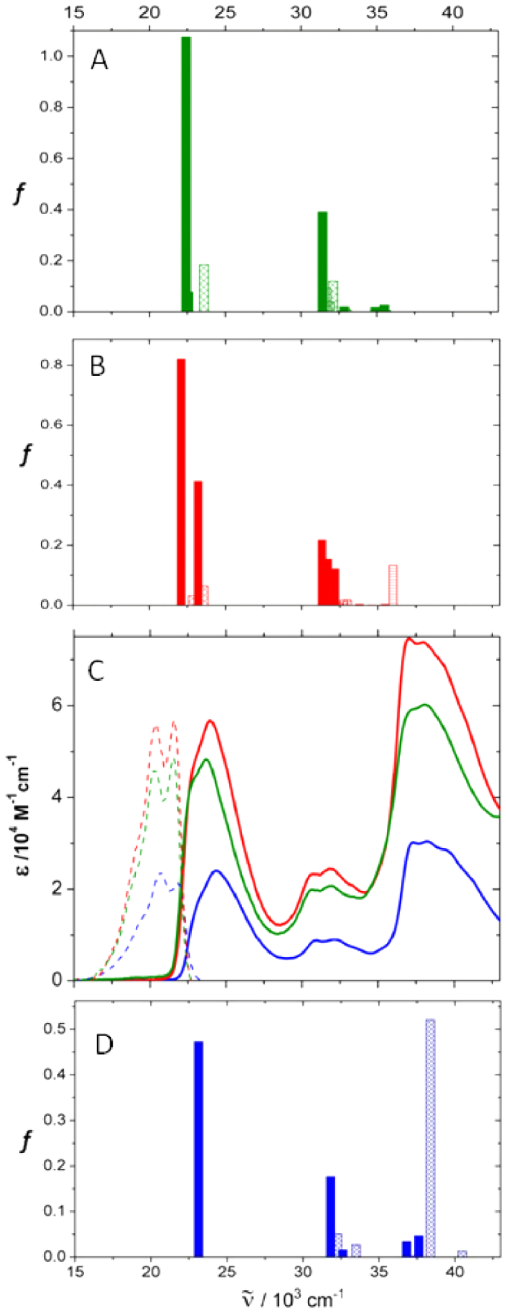

Figure 1. UV−vis absorption (solid lines) and fluorescence (dashed lines, normalized to absorption) of **1**−**3** in AN. Color-coded calculated spectra are displayed above (**2** and **3**) and below (**1**).

quantum yields Φ_T (Table 2). In any solvent, the spectrum of **1**,[16] also shown in Figure 2, is only observable upon sensitization. The spectra of **2** and **3** contain a Gaussian band near 21.5 × 10^3 cm^{-1} and a weak broad feature peaking near 14 × 10^3 cm^{-1}. From ground state depletion, the peak molar extinction coefficient for the former is 34 × 10^3 and 37 × 10^3 M^{-1} cm^{-1} for **2** and **3**, respectively, and can be compared with the value of 32.1 × 10^3 M^{-1} cm^{-1} reported[16] for **1**. Negative peaks near 24 × 10^3 cm^{-1} are due to ground state depletion.

The lifetimes of the triplets of **2** and **3** in various solvents are reported in Table 2. These lifetimes were determined at low concentration from a single exponential fit to the data. At higher concentration, the decay of the triplet becomes nonexponential. The lifetimes of both **2** and **3** at concentrations

dx.doi.org/10.1021/jp310979q | J. Phys. Chem. B 2013, 117, 4680−4695

Table 2. Steady-State Photophysical Data for 1,[16] 2, and 3 in Solution[a]

cmpd.	solvent	$\tilde{\nu}_{ABS}/10^3$ cm^{-1}	$\Gamma_{ABS,0-1}$	$\tilde{\nu}_F/10^3$ cm^{-1}	$\Gamma_{F,0-1}$	Φ_F	k_{F1}/ns^{-1}	k_{F2}/ns^{-1}	Φ_T	$\tilde{\nu}_{T-T}/10^3$ cm^{-1}	k_T ms^{-1}
1	CH	24.33 ± 0.03	0.69 ± 0.04	22.32 ± 0.03	0.66 ± 0.02	0.95 ± 0.03	0.154 ± 0.008		<0.01 ± 0.005	22.12 ± 0.06	6.8 ± 0.5
	AN	24.36	0.71	22.12	0.57	0.98	0.132		<0.01	22.08	3.9
	DMSO	24.04	0.59	21.83	0.60	0.97	0.175		<0.01	21.98	5.4
	DMF	24.15	0.66	22.03	0.61	0.96	0.147		<0.01	22.03	4.2
2	CH	23.77	0.43	21.92	1.14	0.97	0.218		<0.01	21.75	4.3
	AN	23.72	0.77	21.60	1.06	0.19	0.518 ± 0.1 (0.58)	4.50 ± 0.4(0.42)	0.012	21.55	5.3
	DMSO	23.42	0.71	21.60	1.45	0.13	1.23 (0.76)	4.65 (0.24)	0.026	21.30	5.0
	DMF	23.57	0.48	21.61	1.40	0.27	0.469(0.60)	7.46 (0.40)	0.023	21.45	5.8
3	CH	23.57	0.74	21.78	1.16	0.92	0.254	-	<0.01	21.60	5.9
	AN	23.61	0.89	21.55	1.07	0.32	0.581(0.76)	6.67 (0.24)	0.025	21.40	5.6
	DMSO	23.24	0.61	21.47	1.40	0.17	0.398(0.64)	7.46 (0.36)	0.057	21.25	4.7
	DMF	23.40	0.55	21.41	1.25	0.32	0.592(0.70)	7.81 (0.30)	0.049	21.30	5.3

[a]Peak location in ground state absorption $\tilde{\nu}_{ABS}$, in corrected fluorescence $\tilde{\nu}_F$, and in triplet absorption $\tilde{\nu}_{T-T}$; the ratio of intensities of the first to the second peak in absorption $\Gamma_{ABS,0-1}$ and corrected fluorescence $\Gamma_{F,0-1}$ obtained from fitting of the former with three and the latter with four Gaussians; the fluorescence quantum yield Φ_F, triplet quantum yield Φ_T, fluorescence rate constants k_{F1} and k_{F2}, and the rate constant of triplet decay k_T. Relative amplitudes for rate constants k_{F1} and k_{F2}, where both are necessary for the fit, are shown in parentheses.

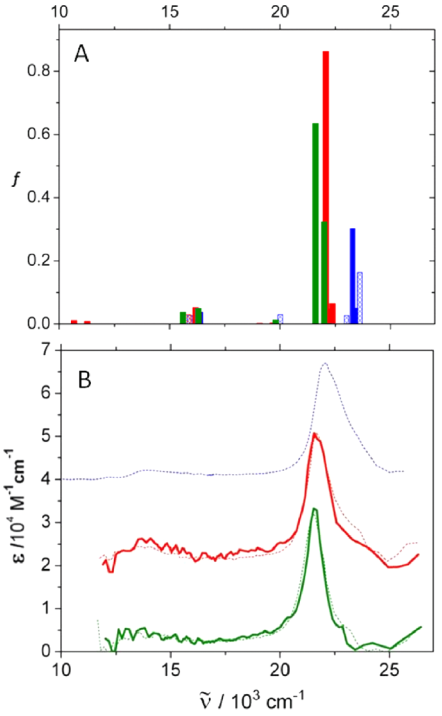

Figure 2. Direct (color) and sensitized (dotted) photoinduced T_1-T_n absorption spectra of **1**−**3** in DMSO at delay times longer than 100 μs. Color-coded calculated spectra are shown above.

below 10 μM are 220 ± 20 μs, while at concentrations above 50 μM, a faster component with a concentration-dependent decay time of less than 50 μs is apparent, presumably due to triplet−triplet annihilation.

Triplet quantum yield was determined in a series of solvents of varying polarity. Without sensitization, Φ_T of **1** is at or below our instrumental sensitivity (~0.5%) in all solvents,[16] whereas for **2** and **3** this is only true in nonpolar solvents. In polar solvents, Φ_T of **2** and **3** exceeds 1%, and at 300 K the value for **3** is roughly twice that for **2**. The highest yield was observed for **3** in DMF at 230 K and equaled ~9%. The triplet photoproduction action spectra of **2** and **3** in DMSO are shown in Figure 3 and follow the absorption spectra faithfully.

Short-Lived Transients. Whereas in **1** the excited singlet S_1 is the only short-lived transient in solvents of any polarity, the behavior of the dimers **2** and **3** is similarly simple only in nonpolar solvents, where their fluorescence decays are monoexponential. Their 4−5 ns lifetimes in such solvents (Figure 4A) are slightly shorter than the monoexponential 6−7 ns lifetimes of the monomer **1** in solvents of any polarity.[16]

In polar solvents, we find an additional short-lived transient from both **2** and **3**. We describe first the room-temperature results and then examine their temperature dependence.

Time-Resolved Emission from S_1. In polar solvents, the fluorescence decays of **2** and **3** cannot be fitted with a single exponential rate constant (Figure 4B), instead requiring two exponential components for a satisfactory fit (Tables 2 and 3). The components vary in a systematic fashion with solvent, with the faster decays decreasing in amplitude as solvent polarity decreases.

Time-Resolved Absorption. The photoinduced absorption and bleaching of **2** and **3** were measured as a function of pump−probe delay from 100 fs to 8 ns. The raw kinetic data were fitted globally to determine rate constants for formation

dx.doi.org/10.1021/jp310979q | J. Phys. Chem. B 2013, 117, 4680−4695

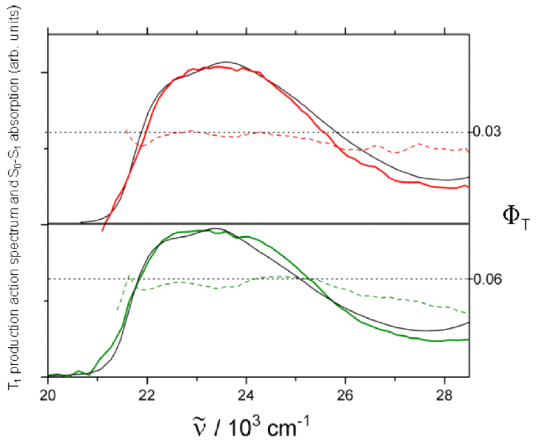

Figure 3. Direct excitation triplet production action spectra in DMSO compared with the absorption spectra (black) for **2** and **3** in DMSO. Dashed line is T_1-T_n signal divided by the S_0-S_1 absorption, normalized such that the value at 24 000 cm^{-1} equals the measured triplet quantum yield.

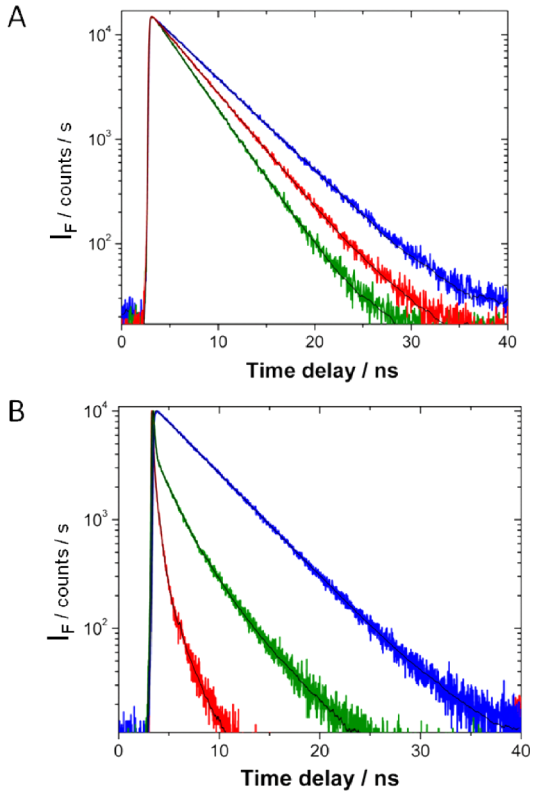

Figure 4. Fluorescence decay traces of **1**–**3** in (A) cyclohexane and (B) DMSO.

and decay of various species, as well as the species associated difference spectra. As reported previously,[16] in the probe wavelength range 22 000–14 000 cm^{-1} the transient absorption spectrum of **1** in all solvents is characterized fully by stimulated S_1-S_0 emission and S_1-S_n singlet absorption with a peak at 14.5×10^3 cm^{-1} with an absorption coefficient of very roughly 20×10^3 $M^{-1}cm^{-1}$. This behavior is mimicked faithfully by **2** and **3** in nonpolar solvents, where **2** and **3** exhibit an instrument-limited rise of stimulated emission and excited singlet absorption, the decays of which can be fitted with an exponential function with rate constants displayed in Table 3.

Table 3. Rate Constants (ns^{-1}) Derived from Compartmental Analysis of Spectrotemporal Data[a]

solution	T	k_F	k_{ET}	k_{BET}	k_{NR}	k_T	k_Y	k_{YX}
2 DMSO	RT	0.23	1.8	2.8	1.1	0.04	n/a	n/a
3 DMSO	RT	0.25	3.8	4.9	0.84	0.08	~0	
3 DMSO	425 K	0.25	14	16	0.84	0.08	16	13
2 CH	RT	0.20						
3 CH	RT	0.22						

[a]RT = room temperature; n/a = not applicable. Error limits: ~10% except for k_{NR} and k_F, which show some covariance and an error limit of ~20%.

The first in a series of S_1-S_n absorption peaks appears at 21×10^3 and 20.5×10^3 cm^{-1} in **2** and **3**, respectively, close to the location of the strongest S_1-S_n peak in **1** (Figure 5). Its

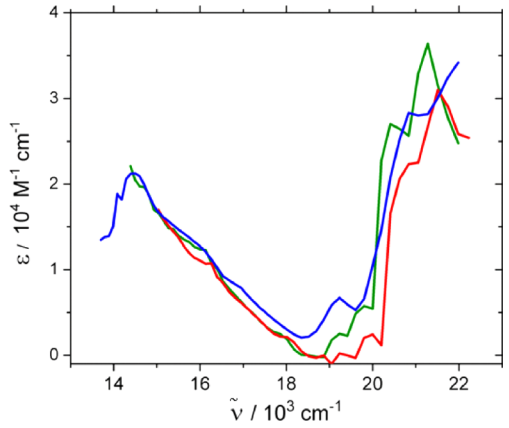

Figure 5. S_1-S_n absorption spectra for **1**–**3** in DMSO extracted from global fit.

absorption coefficient is 30 (**2**) and 34×10^3 M^{-1} cm^{-1} (**3**), comparable to the value reported for **1**. S_1-S_n absorption bands at higher (above 22 000 cm^{-1}) and lower (below 15 000 cm^{-1}) energies are also observed, but the peak positions cannot be accurately measured since they lie outside the range of detection. In polar solvents, the transient absorption spectra are complicated by the appearance of a short-lived nonemissive intermediate **X** that appears to form from the initially excited S_1 state on a sub-nanosecond time scale and to be transformed subsequently into the triplet T_1 on a nanosecond scale. At elevated temperatures, an additional nonemissive intermediate **Y** appears in **3** (but not in **2**), as discussed further below.

The results of time-resolved absorption measurements were fitted to a kinetic scheme depicted in Figure 6 using global target analysis. The processes involved in this scheme after photoexcitation are fluorescence from the nonpolar monomer-like singlet S_1 to the ground state, transfer of population back and forth between S_1 and the intermediate state **X**, nonradiative decay of **X** to S_0, and the formation of the triplet T_1 from **X**, where the disappearance of a single molecule of **X** could cause the appearance of one (intersystem crossing) or two (singlet fission) triplet excitations T_1 in the same dimer molecule. In the case of **3**, at elevated temperatures, the conversion of a fraction of S_1 into **Y** and the subsequent decay of **Y** into **X** are also included. Values obtained for the rate constants, defined in Figure 6, are displayed in Table 3.

The resulting species associated difference absorption spectra of **2** and **3** obtained at room temperature, where **Y** is not

dx.doi.org/10.1021/jp310979q | J. Phys. Chem. B 2013, 117, 4680–4695

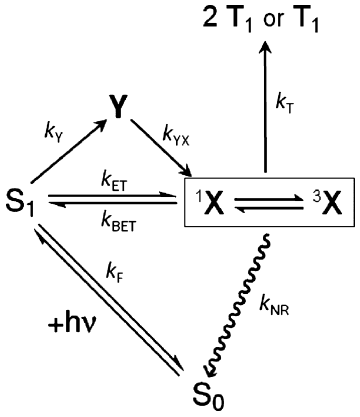

Figure 6. Kinetic scheme used for global target analysis of transient absorption of **2** and **3** in polar solvents.

observed, are plotted in Figure 7, and the associated decay kinetics are shown in Figure 8. The S_1-S_n absorption spectra are also shown separately in Figure 5. The intermediate species **X** is associated with transient absorption bands near 18.5×10^3 and 14.8×10^3 cm^{-1}. These absorptions rise with a time constant of ~250 ps (**2** in DMSO) or ~150 ps (**3** in DMSO), which correlates with the decay of excited state absorption due to S_1, strongly suggesting that **X** is formed from S_1. The absorption by **X** decays with 0.9 ns (**2**) or 1.2 ns (**3**) time constants. The decay of this signal is correlated with the rise of T_1 absorption features, leaving little doubt that T_1 is formed from **X**.

Temperature Dependence of the Fluorescence Quantum Yield. The fluorescence yield Φ_F in DMF was examined as a function of temperature. The compounds were not readily soluble in glass-forming solvents, and the lower end of the temperature range was limited by the solvent freezing point. The data points displayed were obtained by integrating a band near the peak of the fluorescence spectrum. The fluorescence line shapes broaden slightly with increasing temperature, but there is no noticeable peak shift. Going from high to low temperatures, Φ_F of **2** and **3** decreases strongly to a minimum near 300 K, before increasing again between room temperature and the solvent freezing point.

The Φ_F values obtained above 300 K were converted to values of the equilibrium constant K_{eq} for the interconversion of S_1 and **X**, assuming that only S_1 and **X** excited states are populated. As at these temperatures, the interconversion is fast compared with the radiative decay rate, K_{eq} is equal to the ratio $(1 - [S_1])/[S_1]$, determined from Φ_F of fluorescence from S_1, measured in the steady state (Figure 9A). A plot of ln K_{eq} against $1/T$ is linear in the high temperature region, and its slope yields ΔG^0 values of 1.7 kcal/mol (**2** in DMSO), 1.9 kcal/mol (**3** in DMSO), 2.4 kcal/mol (**2** in DMF), and 4.6 kcal/mol (**3** in DMF) with uncertainties on the order of 5%, judging by fit errors. At lower temperatures, the interconversion of S_1 and **X** slows. The S_1 to **X** transition becomes irreversible, and equilibrium is not reached. The excited state reaction then enters a kinetic regime, in which an Arrhenius-like dependence of the rate k_{ET} on temperature is expected.[41] Fitting the data below 250 K produced activation energy values in DMF of E_a = 6.1 kcal/mol for **2** and 4.9 kcal/mol for **3**. The error estimated for these steady-state values is on the order of 25% because the low-temperature end of the curve is not quite linear. The values thus are in reasonable agreement with those derived from

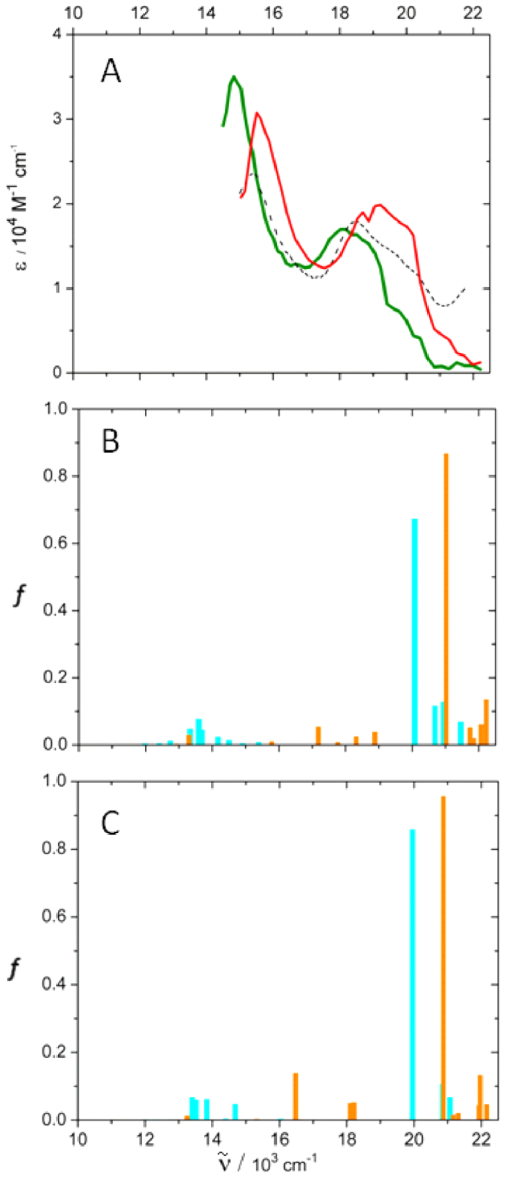

Figure 7. Species associated decay spectra resulting from global target analysis for **2** (red) and **3** (green) in DMSO at room temperature (A). The black dashed line is the sum of the absorption spectra of the radical cation and radical anion of **1**.[16] Calculated transitions for the radical cation (orange) and anion (light blue) of **2** and **3** are shown in B and C, respectively.

transient absorption measurements described in the next section. It is expected that the thermally activated behavior is complicated at low temperatures because the solvent viscosity becomes nearly infinite, causing charge transfer to be severely hindered. The intersection of the fit lines for low and high temperature produces a crossing temperature T_c, at which $k_{ET} = k_{NR}$. It is about 260 K for both **2** and **3**.

Temperature Dependence of Transient Absorption. Ultrafast transient absorption of **2** and **3** was measured in DMSO and DMF. Results for **3** in DMSO probing exclusively the kinetics of **X** are shown as function of temperature in Figure 10A. The logarithm of the rate constant k_{ET} for **2** and **3** in DMF is plotted against $1/T$ in Figure 10B. For **2**, the activation energy for the formation of **X** from S_1 is 2.7 kcal/mol and log A is 11.4, and for **3**, the values are 3.0 kcal/mol and 11.8 (A is the frequency factor in S^{-1}), with an estimated 10% error. These

dx.doi.org/10.1021/jp310979q | J. Phys. Chem. B 2013, 117, 4680−4695

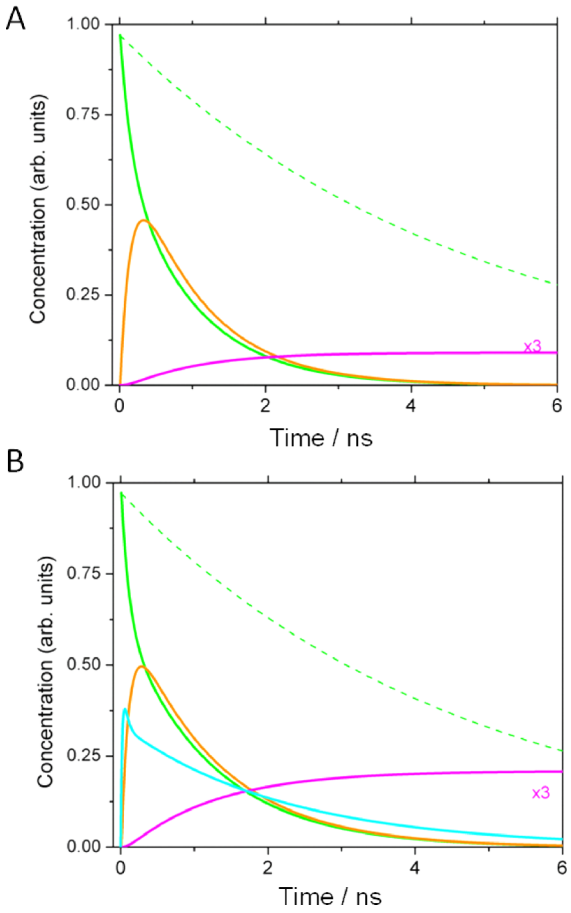

Figure 8. Concentration vs time traces for **2** (A) and **3** (B) in DMSO from the rate constants deduced from global fitting of room-temperature results, assuming initial population only in the S_1 state. Light green: S_1; orange: **X**; magenta: T_1, light blue: **Y**. The dashed green line is S_1 decay in CH.

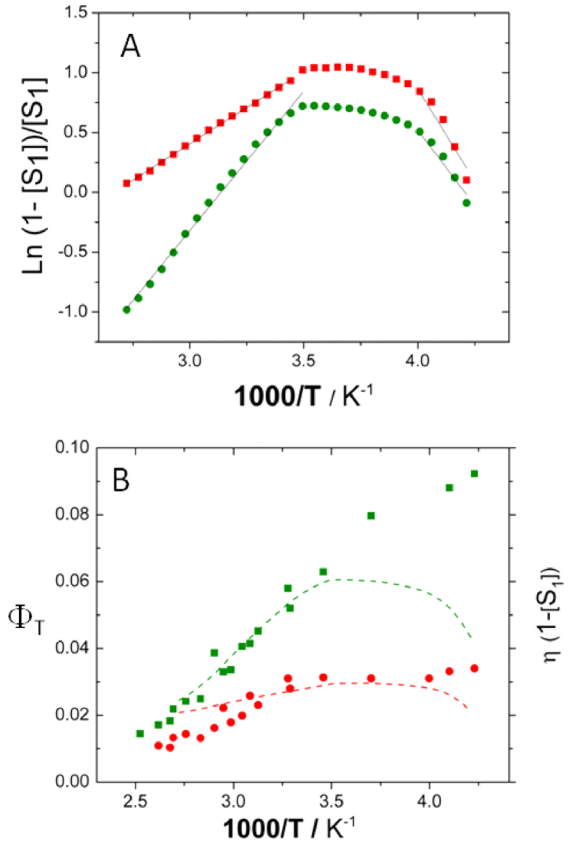

Figure 9. Inverse temperature dependence for **2** (red) and **3** (green) in DMF. (A) $(1 - [S_1])/[S_1]$; solid lines are linear fits in the low and high temperature regimes (see text). For **2**, squares, and for **3**, circles. (B) Φ_T; dashed lines show $\eta(1 - [S_1])$, where η is the efficiency of the conversion of **X** into T_1, estimated from time-resolved spectroscopy. For **2**, circles, and for **3**, squares.

numbers agree within error limits with those derived above from steady state measurements. The rate constants of fluorescence and nonradiative decay are independent of temperature within the experimental accuracy of about 20%.

Temperature Dependence of the Triplet Yield. Figure 9B shows Φ_T as a function of temperature for **2** and **3** in DMF. Since T_1 is formed from **X**, Φ_T is a function of [**X**], which itself changes with temperature; the temperature dependence of the scaled $S_1 - \mathbf{X}$ equilibrium constant, approximated by $\eta(1 - [S_1])/[S_1]$, is also shown for comparison (dashed lines). Here, η is the efficiency of the conversion of **X** into T_1, which is estimated below to be 0.04 for **2** and 0.09 for **3**. The agreement between Φ_T and the scaled equilibrium constant is quite good except for temperatures below about 275 K, where Φ_T continues to rise while the equilibrium constant for the conversion of S_1 into **X** reaches a plateau and subsequently decreases. This deviation is more pronounced for **3** than for **2**.

All results described up to now were qualitatively similar for **2** and **3**. Next, we describe the only instance where the two dimers differ strikingly. For **2** in DMSO at temperatures above ~360 K, the decay of **X** remains monoexponential, and the system still follows the scheme described in Figure 6 and in eq. S2 without the intervention of **Y**. However, under these conditions, for **3** the transient absorption so far attributed solely to **X** develops a new faster decay component and becomes biexponential (cf. the light blue trace in Figure 8B). Global analysis of the spectrotemporal data shows that at these temperatures two species with different but strongly overlapping spectra (Figure 11), different decay times, and indistinguishable rise times, equal to the decay time of S_1, contribute to the absorption in the 14000−19000 cm^{-1} region. The fit was based on an expanded version of the kinetic equation system S2 (Supporting Information), to which the formation of an additional species **Y** from S_1 and its decay to T_1 have been added. **Y** decays in less than 500 ps, leaving the remaining transient population **X** to decay on a 2−3 ns time scale. Due to severe spectral overlap and the small amount of T_1 present, the concentration of T_1 cannot be monitored until the other transients have decayed and we cannot tell whether its rise is biexponential. The primary fate of **Y** appears to be conversion into **X**, since its decay does not produce a clear recovery of S_1 or S_0. The other contributing species is the already known **X**, based on its spectrum and rise and decay times. Clearly, although **X** and **Y** are formed from S_1 in competition with each other, they are not in fast equilibrium.

Like the absorption spectrum of **X**, that of **Y** also contains a peak attributable to the radical cation and a peak attributable to a radical anion of the chromophore **1**, but they are somewhat shifted and present in a different intensity ratio. The observed ratio [**Y**]/[**X**] increases with temperature, and just below the DMSO boiling point the absorbance due to **Y** is responsible for roughly 40% of the total. The ratio of **Y** to **X** and the rise times of both are independent of the concentration of **3** in the

dx.doi.org/10.1021/jp310979q | J. Phys. Chem. B 2013, 117, 4680−4695

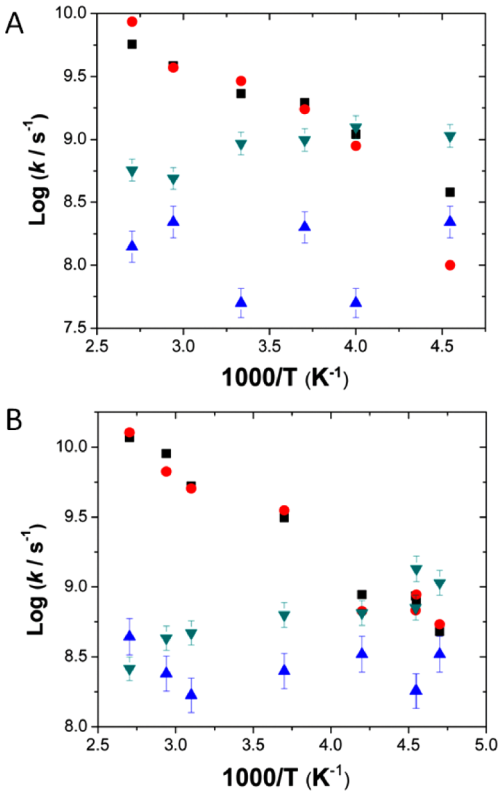

Figure 10. Temperature dependence of transient decay rate constants for **2** (A) and **3** (B) in DMF. Color code: red circles, k_{ET}; black squares, k_{BET}; green diamonds, k_{NR}; blue triangles, k_F.

solution in the 5−75 μM range, limited by the absorbance range appropriate for achieving reasonable signal in transient absorption experiments. DOSY NMR measurements provided no indication that **3** is aggregated in the solution.

Pulse Radiolysis of 3. The absorption spectra of the radical cation and radical anion of **3** were obtained by pulse radiolysis in 1,2-dichloroethane and THF, respectively, and are shown in Figure 11A.

DISCUSSION

Electronic States. Given the prior knowledge of the electronic states of the monomer **1**,[16] the locally excited states of the covalent dimers obtained from experiment or calculation contain no surprises. There is every reason to believe that the excitation, or the charge and spin, are well localized on one side of the molecule, and that the potential energy barriers for their transfer to the other half are very small.

The main conclusion from Table 1 is that in a nonpolar medium, the calculated excitation energy of the S_1 state is only slightly lower than twice that of the T_1 state, which in turn is essentially identical with that of the double triplet states (TT), while charge-transfer states (CA) lie far higher. In DMSO, the situation is similar, except that now the excitation energy of the CA states is similar to those of the S_1 and TT states. Although the DFT calculated T_1 excitation energy of **1** is a little higher than half the S_1 energy, experimentally the two are approximately equal,[16] and this is likely to be true for **2** and **3** as well. As far as state energies go, the conditions for efficient singlet fission in these covalent dimers are met, and it would be approximately thermoneutral.

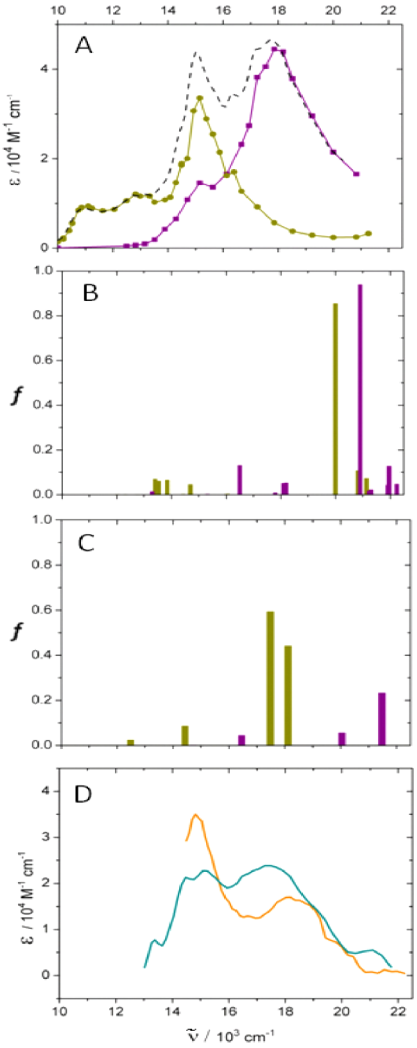

Figure 11. (A) Absorption spectra of the radical cation (**3C**, purple, squares) and anion (**3A**, dark yellow, circles) of **3** in 1,2-dichloroethane and THF, respectively, and their sum (dashed line). (B) Calculated transitions for **3C** (purple) and **3A** (dark yellow). (C) Calculated transitions in the charged fragments of **3** at a geometry twisted next to the furan ring, the radical cation of 1-phenylisobenzofuran (purple) and radical anion of 1-(tetramethyl-*p*-biphenylyl)-3-phenylisobenzofuran radical anion (dark yellow), at their optimized geometries. (D) Transient absorption spectra of **X** (orange) and **Y** (cyan), formed from **3** in DMSO.

There is nothing unusual about the observed or the TD-DFT calculated absorption spectra of the various states, and the comparison of the two is very satisfactory for the neutral states as long as the artifactual charge-transfer states are dismissed, as discussed above. Since the interaction between the two chromophores in the dimers is feeble, allowed vertical transitions from the symmetric structures, allowed for S_0-S_1 and Q_1-Q_n and forbidden for S_0-T_1, are expected to be nearly the same as in the S_0-S_1, T_1-T_n, and S_0-T_1 spectra of **1**, respectively, but with twice the molar intensity. Electronic transitions occur in nearly degenerate pairs of in-phase and out-of-phase excitation in the two chromophores. The in-phase transitions should be polarized in the 2-fold symmetry axis and the out-of-phase transitions perpendicular to it.

The T_1-T_n and S_1-S_n spectra of the dimers should resemble the sums of the T_1-T_n or S_1-S_n spectrum of the monomer **1**

dx.doi.org/10.1021/jp310979q | J. Phys. Chem. B 2013, 117, 4680−4695

with its S_0-S_n spectrum, and they do. The transitions that correspond to T_1-T_n or S_1-S_n excitations should be polarized approximately along the local short (z') or long (y') in-plane axis of the excited chromophore, and those that correspond to S_0-S_n excitations should be polarized along the local short (z'') or long (y'') in-plane axis of the ground-state chromophore. In the UV region where the S_0-S_n spectrum of **1** is intense, observation of T_1-T_n and S_1-S_n spectra was not possible, but the observed parts of the T_1-T_n and S_1-S_n spectra look nearly the same in **1**–**3**, as expected. The minor differences in the intensities of the three vibrational components of the first transition are probably related to the presence of more than one conformation, due to the ambiguity in the sense of twisting of the aryl substituents on the isobenzofuran rings.

Nonpolar Solvents. In nonpolar solvents, the photophysical behavior of the dimers **2** and **3** is extremely simple and essentially identical to that of the monomer **1** in any solvent. Fluorescence is virtually the only fate of the initially excited S_1 state. There is no indication that S_1 is converted to T_1, either by singlet fission or by intersystem crossing. The latter would not be expected, since it does not take place in **1**. We are forced to conclude that the degree of coupling between the two chromophores **1** in the dimers **2** and **3** is insufficient to permit singlet fission to compete successfully with emission, whose rate constant is 0.22 (**2**) or 0.25 (**3**) ns^{-1}. Since a 1% triplet yield would have been detected, we conclude that in a nonpolar environment, and starting with a localized singlet excitation, the rate constant for singlet fission in the dimers **2** and **3** is less than 2.2 and 2.5 μs^{-1}, respectively. This contrasts starkly with the ~40 ns^{-1} rate constant observed in neat solid **1**, and is reminiscent of the observations that were made for covalent dimers of tetracene.[17,18]

There could be various reasons for the much smaller rate constant for singlet fission in the dimer than in the solid. For instance, the higher dielectric constant in the solid stabilizes virtual charge-transfer states, the ability of the triplets to diffuse apart in the solid provides an entropic driving force for their formation, and the likely delocalization of the initial excited state over several chromophores might be somehow favorable even though this does not follow from inspection of the relevant matrix elements.[1] However, the most likely source of the small rate constant for singlet fission in the covalent dimers is poor coupling between the individual chromophores **1** due to inappropriate geometrical relation between them. Sensitivity to this factor has been noted in the work with thin polycrystalline films of neat solid **1**, in that triplet yields observed for different crystal modifications can differ by an order of magnitude.[15]

In a crystal of **1**, the neighboring molecules are slip-stacked, and inspection of the expressions for the matrix elements for both the direct and the mediated contribution to singlet fission reveals this to be a highly desirable arrangement[1,42] (other relations between neighbors are also present and are presumably less effective). The arrangement in **2** and **3**, and also in the previously examined covalent dimers of tetracene,[17,18] is very different, and is easily seen to be unfavorable.

In the first approximation, the electronic matrix element whose square enters into the rate expression contains a sum of two terms. The first "direct" term contains only contributions from the two-electron part of the Hamiltonian H,

$$\langle {}^1(\mathrm{TT})|H|\mathrm{S_1S_0}\rangle = (3/2)^{1/2}[(l_\mathrm{A}l_\mathrm{B})||(l_\mathrm{A}h_\mathrm{B}) - (h_\mathrm{A}h_\mathrm{B})||(h_\mathrm{A}l_\mathrm{B})] \quad (1)$$

Here, $(l_\mathrm{A}l_\mathrm{B})||(l_\mathrm{A}h_\mathrm{B})$ stands for the two-electron repulsion integral between the overlap density formed by the multiplication of the LUMO on partner A (l_A) with the LUMO on partner B (l_B) and the overlap density formed by the multiplication of l_A with the HOMO on partner B (h_B), and the definition of $(h_\mathrm{A}h_\mathrm{B})||(h_\mathrm{A}l_\mathrm{B})$ is similar. Even in the best of cases, this term is generally small because the partners A and B are separated in space, their molecular orbitals hardly overlap at all, the overlap densities are minute, and their mutual repulsion usually negligible. In **2** and **3**, the overlap of molecular orbitals located on one and the other half of the molecule, the partners A and B, is especially small, and the contribution from the direct term must be almost exactly zero.

The second "mediated" term originates in mixing with the charge-transfer states ^{1}(CA) and ^{1}(AC), and we believe it to be dominant in most cases of singlet fission:[42]

$$-\langle {}^1(\mathrm{T_1T_1})|H|\mathrm{CA}\rangle[\langle {}^1\mathrm{CA}|H|\mathrm{S_1S_0}\rangle + \langle {}^1\mathrm{AC}|H|\mathrm{S_1S_0}\rangle]/\Delta E \quad (2)$$

where ΔE is the energy difference between the degenerate charge-transfer states and the nearly degenerate S_0S_1 and ^{1}(TT) states. Now, both the one-electron and the two-electron parts of H contribute

$$\langle {}^1\mathrm{TT}|H|\mathrm{CA}\rangle = (3/2)^{1/2}[\langle l_\mathrm{A}|F|h_\mathrm{B}\rangle + (l_\mathrm{A}h_\mathrm{B})||l_\mathrm{B}l_\mathrm{B}) - (l_\mathrm{A}h_\mathrm{B})||(h_\mathrm{A}h_\mathrm{A})] \quad (3)$$

$$\langle {}^1\mathrm{CA}|H|\mathrm{S_1S_0}\rangle = \langle l_\mathrm{A}|F|l_\mathrm{B}\rangle + 2(h_\mathrm{A}l_\mathrm{A})||(h_\mathrm{A}l_\mathrm{B}) - (h_\mathrm{A}h_\mathrm{A})||(l_\mathrm{A}l_\mathrm{B}) \quad (4)$$

$$\langle {}^1\mathrm{AC}|H|\mathrm{S_1S_0}\rangle = -\langle h_\mathrm{A}|F|h_\mathrm{B}\rangle + 2(h_\mathrm{B}l_\mathrm{B})||(h_\mathrm{A}l_\mathrm{B}) - (l_\mathrm{B}l_\mathrm{B})||(h_\mathrm{A}h_\mathrm{B}) \quad (5)$$

where F is the Fock operator.

To obtain qualitative insight, we neglect the two-electron part, in which case the mediated term can be written as

$$-(3/2)^{1/2}\langle l_\mathrm{A}|F|h_\mathrm{B}\rangle[\langle l_\mathrm{A}|F|l_\mathrm{B}\rangle - \langle h_\mathrm{A}|F|h_\mathrm{B}\rangle]/\Delta E \quad (6)$$

Upon expansion of the orbitals l and h in atomic orbitals, recognition of the chemical identity of partners A and B, and introduction of the tight-binding approximation, this simplifies to

$$(3/2)^{1/2}c_hc_l(c_h^2 - c_l^2)\beta_{\mathrm{CC}}^2/\Delta E \quad (7)$$

where β_{CC} is the resonance (hopping) integral across the junction between the two halves of the dimer, i.e., between the carbon $2p_z$ atomic orbitals of the two partners at the junction that participate in their frontier orbitals, and c_h and c_l are the amplitudes of HOMO and LUMO at these atomic orbitals. This quantity must be clearly small, for several reasons: (i) the large energy difference ΔE between the S_1 and the charge transfer states (Table 1), (ii) the relatively small amplitude c_h of the HOMO and c_l of the LUMO at the junction points, (iii) the cancellation of the squares of the expansion coefficients c_h^2 from the HOMO and c_l^2 from the LUMO (because of the pairing theorem for alternant hydrocarbons, these squares are equal in tetracene; they will be close to equal even in **1**), and last but not least, (iv) the small magnitude of β_{CC}^2. In **2**, where the carbon atoms at the junction are connected through a CH_2 group, β_{CC} only reflects the effects of hyperconjugation through this group. In **3**, the junction carbons are connected directly, but the two π systems are twisted nearly orthogonal and β_{CC} must again be small. Clearly, linking the two halves of a covalent dimer symmetrically end-to-end, as has been done

dx.doi.org/10.1021/jp310979q | J. Phys. Chem. B 2013, 117, 4680–4695

here and in the earlier work with tetracene,[17,18] is far from optimal if fast singlet fission is the objective. However, at least the choice of the linking point is somewhat favorable, since for most other choices the coefficients c_h and c_l are even smaller.

Polar Solvents. The novelty offered by the dimers **2** and **3** is in their photophysics in polar solvents, where in both cases S_1 is in rapid equilibrium with an intermediate **X**. An intriguing puzzle is provided by the observation that at elevated temperatures the S_1 state of the dimer **3** also produces an additional intermediate **Y**, while that of the otherwise extremely similar dimer **2** does not. In the following, we focus on these aspects of the results.

From the temperature dependence of the equilibrium constant for the interconversion of **X** with S_1, the former is 1.5−4.5 kcal/mol below the latter. Since **X** and **Y** only appear in polar solvents, an immediate suspicion is that they are dipolar species produced by electron transfer from one to the other chromophore within the dimer, stabilized by twisting[43] and asymmetric solvation. Intramolecular charge transfer in weakly coupled (usually twisted) dimers is well precedented, for instance in the classical case of 9,9′-bianthryl.[44]

The assignment of **X** as a charge-transfer species, in which the donor and the acceptor are of equal size, separated by the central covalent junction in the molecule, and hence both equal to **1**, is confirmed beyond reasonable doubt by comparison of peak positions and intensities in its absorption spectrum with those of the radical cation and the radical anion of the monomer **1**, which were reported previously[16] (Figures 7 and 11). Within the observed region, the radical cation of **1** has a single strong peak at 18.5×10^3 cm^{-1} (ε_{max} = ∼17.8×10^3 $M^{-1}cm^{-1}$) and its radical anion has an even stronger single peak at 15.2×10^3 cm^{-1} (ε_{max} = ∼23.5×10^3 $M^{-1}cm^{-1}$). The spectra of the radical cation and radical anion of **3**, reported presently, are very similar to those of the radical ions of **1**, but are more intense. The radical cation of **3** peaks at ∼17.9×10^3 cm^{-1} (ε_{max} = ∼44.5×10^3) and the radical anion of **3** at ∼15.2×10^3 cm^{-1} (ε_{max} = ∼33.5×10^3).

The spectra of **X** contain two intense peaks in the same region, and their positions and intensities agree very well with those expected for the sum of the spectra of the radical cation and the radical anion. They occur at 15.5×10^3 cm^{-1} (ε_{max} = 30×10^3 $M^{-1}cm^{-1}$) and 19.2×10^3 cm^{-1} (ε_{max} = 20×10^3 $M^{-1}cm^{-1}$), respectively, for **2**, and at 15.0×10^3 cm^{-1} (ε_{max} = 34×10^3 $M^{-1}cm^{-1}$) and 18.4×10^3 cm^{-1} (ε_{max} = 17×10^3 $M^{-1}cm^{-1}$), respectively, for **3**. The spectra of **X** formed from **2** and **3** thus differ only by minor shifts, and their sum is nearly exactly equal to the sum of the spectra of the radical ions for both **2** and **3** (Figure 7A).

In contrast to the spectra calculated by the TDDFT method for the uncharged states, those calculated for the radical ions of **1**−**3** agree with observations only qualitatively, in that a single intense peak is predicted in each, but its excitation energy is too high by $2-3 \times 10^3$ cm^{-1} in the case of the radical cation and by $4-5 \times 10^3$ cm^{-1} in the case of the radical anion. A similar discrepancy was noted earlier for the radical ions derived from **1**.[16] If one approximates the calculated absorption spectrum of **X** by the sum of the spectra calculated for its radical cation constituents, an agreement with experiment is reached only if one assumes that similar empirical corrections need to be made as for the monomeric radical ions, and this is entirely reasonable.

The spin state of the dipolar species **X** is not apparent from its visible spectrum, since the absorption spectra of the dipolar singlet ^{1}**X** and triplet ^{3}**X** are expected to be very similar. The absorption spectrum attributed to **X** might actually be due to a mixture of ^{1}**X** and ^{3}**X**, or exclusively to one or the other. Since the intermediate is nonemissive as nearly as we can tell, we cannot use fluorescence for a differentiation. However, the normal values of the frequency factor for the rates of the formation of **X** from S_1 in **2** and **3**, about 10^{12}, leave no doubt that when first formed, **X** is in its singlet state ^{1}**X**. The frequency factor for the reverse reaction is also roughly 10^{12} and the rapid equilibration between S_1 and **X** is certainly compatible with the notion that the bulk of the dipolar species is present as ^{1}**X** throughout. Its conversion to T_1 thus requires a multiplicity change. This could occur by the usual spin−orbit coupling-induced intersystem crossing or by going through the second phase of two-step singlet fission.

It is clear from the experimental results and also from calculated energies (Table 1) that opportunities for singlet fision are improved in polar solvents. The improvement is not large for the one-step process, since the value of ΔE in the denominator in expression 7 refers to virtual charge-transfer states, which are stabilized by a solvent that is more polarizable but offer no time for solvent reorientation and therefore are not stabilized by solvent polarity. The relevant ΔE is therefore nowhere near zero as Table 1 might otherwise suggest. However, the two-step singlet fission process, which proceeds through a real intermediate that can take full advantage of solvent polarity, now becomes feasible. The observation that the dipolar intermediate is indeed formed rapidly makes it clear that the electronic matrix elements for the initial charge transfer, $\langle {}^1\mathrm{CA}|H|\mathrm{S_1S_0}\rangle$ or $\langle {}^1\mathrm{AC}|H|\mathrm{S_1S_0}\rangle$ (in our approximation, $-(3/2)^{1/2}c_l^2\beta_{CC}{}^2$ or $-(3/2)^{1/2}c_h^2\beta_{CC}{}^2$), have a sufficient magnitude. The question is whether the matrix element for the step in which two triplets are generated from the charge-transfer state, $\langle {}^1\mathrm{TT}|H|\mathrm{CA}\rangle$ (in our approximation, $-(3/2)^{1/2}c_hc_l\beta_{CC}{}^2$), is sufficiently large for this process to be competitive. Since c_l^2, c_h^2, and c_lc_h have the same order of magnitude, this appears to be possible.

In a covalent dimer such as **2** or **3**, where triplets formed by singlet fission cannot diffuse apart, they most likely remain correlated and need to be thought of as superpositions of nine sublevels. If the spin part of the Hamiltonian is neglected, they form the ^{1}(TT), ^{3}(TT), and ^{5}(TT) states. The first two are not the lowest states of their multiplicity and can perhaps decay rapidly by internal conversion, the former into S_0 and possibly also S_1, and the latter to T_1. Thus, even if singlet fission works well and the ^{1}(TT) state is initially produced efficiently, there is no guarantee that much T_1 will be observed in the experiments. The spin part of the Hamiltonian is capable of mixing the singlet, triplet, and quintet sublevels of the double triplet state and may protect some of the triplets formed from decay. These considerations suggest that it would be interesting to examine the effect of outside magnetic field on the kinetics of the **X** to T_1 conversion.

The rate constant of formation of **X** from S_1, k_{ET}, for **2** in DMF and DMSO is considerably smaller than in AN (and to a lesser extent for **3** in AN), a less viscous solvent. In the limit of nonadiabatic charge transfer, a relationship between ΔG^0, $\Delta G^{\ddagger}$ and the reorganization energy λ can be formulated:

$$\Delta G^{\ddagger} = \Delta G^0/2 + \lambda/4 + (\Delta G^0)^2/4\lambda \qquad (8)$$

where ΔG^0 represents the driving force, and $\Delta G^{\ddagger}$ is the effective barrier for the transition. From known values of ΔG^0 and $\Delta G^{\ddagger}$, values of λ can be derived. For **2** and **3** in DMF, the

dx.doi.org/10.1021/jp310979q | J. Phys. Chem. B 2013, 117, 4680−4695

reorganization energies are 7.5 and 4.8 kcal/mol, respectively. Although the charge-transfer process may not be in the fully nonadiabatic regime, values of λ are comparable to those measured for other charge-transfer transitions in covalently bound dimers,[45] suggesting that this zero-order approximation captures the essential reaction dynamics. The larger reorganization energy for **2** may be an indication that the geometry (and possibly dipole moment) of **2** changes more dramatically between S_1 and ^{1}**X** than it does for **3**, necessitating a concomitant change in the solvent configuration. This is consistent with the fact that **2** has more numerous low energy conformers than **3**. An additional contribution may arise from inner-sphere effects, including intramolecular reorganization, although specific vibronic contributions to λ are not included in the previous analysis, and a more extensive study would need to be performed in order to test the full influence that torsional motion might have on the transition rate, as has been concluded in other cases.[46]

The dipolar species **X**, whose bulk is present in the singlet state, is in a thermal equilibrium with S_1. Since its relative amount in the equilibrium increases at low temperatures, it is not surprising that the yield of T_1 increases as temperature is reduced. In the low-temperature limit, the return of **X** to S_1 becomes negligibly slow, and the supply of **X** is dictated by the rate of its formation from S_1. Most of the species **X** returns nonradiatively to the ground state by diabatic back electron transfer, and only a small fraction crosses to the relaxed triplet state T_1. The complex nature of the disappearance of S_1 is reflected in the multiexponential decay of its fluorescence. The three unimolecular processes that depopulate **X** (going to S_1, to S_0, or T_1) compete, but the return to S_0 is the fastest and determines the lifetime. Since neither the rate constant for the disappearance of **X** nor that for the appearance of T_1 shows a temperature dependence, the internal conversion to S_0 is not thermally activated, and this is not surprising, given its exothermic nature that places it in the Marcus inverted region. The triplet yield exhibits a temperature dependence that mimics that of the S_1−**X** equilibrium above about 275 K. However, as the solvent approaches the freezing point, the rate constant for the formation of **X** decreases, presumably due to the slowing rate of solvent motion that must accompany the charge transfer event.

If ordinary intersystem crossing is largely responsible for the triplet formation, the additional temperature dependence of Φ_T not contained in the S_1−**X** equilibrium could be explained by the existence of an equilibrium between ^{1}**X** and ^{3}**X** with only a small fraction of the species in the ^{3}**X** state. The ^{3}**X** species present may have to overcome a thermal barrier to proceed to T_1. The temperature dependence of the T_1 formation rate will then reflect both the difference in the energies of ^{1}**X** and ^{3}**X**, which affects the equilibrium constant, and the activation energy for the ^{3}**X** to T_1 step. There is precedent for intersystem crossing in a similar charge-transfer state.[47,48]

Is any of the triplet produced by singlet fission? In principle, the results of the global analysis can be used to tell whether the decay of one molecule of **X** produces one or two molecules of T_1, if the true yields of **X** and T_1 can be accurately measured versus time. This is difficult because most of the decay of **X** produces S_0. Assuming that S_1 is the only source of **X**, and that fluorescence is the only other decay mode of S_1, the quantum yield of formation of **X** is $1 - \Phi_F$. Assuming that below 360 K, **X** is the only source of T_1, and recognizing that the efficiency η with which T_1 is formed from **X** is $\Phi_T/(1 - \Phi_F)$, we use the known molar absorption coefficient of T_1 to find for **2** in DMSO that each molecule of **X** that disappears produces 0.04 ± 0.02 molecules of T_1. For **3**, the value is 0.09 ± 0.03. The values of the T_1−T_n extinction coefficient and the transient absorption amplitudes (especially of the triplet, with its small relative yield) are the largest source of uncertainty. These values are clearly far below unity and thus do not provide direct information about the possible role of singlet fission in the formation of triplets. Modeling the bleach, decay of **X**, and rise of T_1 versus time assuming either the production of two triplets from a single **X** (singlet fission) or one triplet from a single **X** (ordinary intersystem crossing) does not produce results different enough to decide with certainty which process occurs. Although we find that **2** and **3** are good candidates for the type of two-step singlet fission discussed in the literature,[1] we do not have strong enough evidence for this process to be able to definitely assign any of the triplet yield to singlet fission. Even if the observed triplets originate in singlet fission, their yield is disappointingly small, due to the efficient decay of the dipolar state **X** to S_0.

The transient spectrum of the species **Y** at higher temperatures in **3** (cyan curve in Figure 11D) also contains two strong peaks in the visible region but is quite different from the spectrum of **X** obtained from **3** (dark yellow curve in Figure 11D), most notably by a reversal of the relative strengths of radical cation and radical anion peaks, a red shift of the cation peak, and doubling of the anion peak. It is, however, sufficiently similar to the sum of spectra obtained for the radical cation and anion of **3** by pulse radiolysis (Figure 11A) that an assignment to a free radical ion pair **3C** + **3A** had to be considered. This would have to be formed in an encounter of the dipolar species **X** with a ground state **3**. A diffusive encounter is ruled out by the fast (<100 ps) formation of **Y** even at relatively low concentrations and the concentration independence of its formation rate. A search for ground-state aggregation by diffusion-ordered spectroscopy (DOSY) NMR provided no support for this possibility (Supporting Information).

Somewhat reluctantly, we must conclude that the conversion of S_1 of **3** to **Y** is monomolecular and that **Y** is a conformational isomer of the intramolecular charge-transfer state **X**, whose formation is favored at higher temperatures. The structure of **3** certainly contains a sufficient number of single bonds around which rotation is possible. The absence of **Y** among the transients formed from **2** would then be attributed to an absence of an analogous low-energy conrformational minimum or a higher barrier for its formation from $\mathbf{S_1}$. The rapid decay of **Y** shows that it is not in fast equilibrium with **X**. The decay does not appear to lead to the ground state of **3** since no correspondingly fast component of ground state bleach recovery is seen. The observations are compatible with a decay of **Y** to **X** or possibly T_1 (by singlet fission or ordinary intersystem crossing).

A likely structure of **Y** is suggested by a recent report of twisted intramolecular charge-transfer states of derivatives of **1** substituted in the phenyl ring in polar solvents, in which one of the phenyl rings is twisted orthogonal to the furan ring to which it is attached.[35] TD-DFT calculations of the absorption spectra of the radical ions of the fragments that would result from cutting the conjugated system of **3** between a furan ring and a tetramethylbiphenyl moiety (Tables S5 and S6) showed that the sum of the spectra of a radical cation on the smaller fragment and a radical anion on the larger fragment is compatible with the spectrum observed for **Y** if one makes a

dx.doi.org/10.1021/jp310979q | J. Phys. Chem. B 2013, 117, 4680−4695

similar empirical shift to lower energies as was necessary to reach agreement with the spectrum of **X** (Figure 11). The appearance of two calculated transitions of lower intensity instead of a single intense transition in the radical anion appears to fit the observations and argues against the opposite assignment of charges. However, we make no claim that the structure of **Y** has been established with certainty.

CONCLUSIONS

Triplet formation and decay were observed in dimers of **1** designed to test the coupling strength and energy-level dependence of singlet fission. Triplet quantum yields in the linear dimers **2** and **3** reach ∼9% in polar solutions, much in excess of those observed in monomeric **1** in solution, but far below those observed in neat solid **1**. They depend systematically on solvent and temperature. Clear evidence was obtained for a charge-transfer intermediate in their formation, but it is not certain whether two-step singlet fission or ordinary intersystem crossing is involved when the charge-transfer intermediate is converted to T_1.

We conclude that at least for this chromophore, triplet yield in the weakly coupled linear dimers **2** and **3** is nowhere near 200%, and singlet fission is far too slow to observe at all in a nonpolar solvent and maybe not in a polar solvent either. We have examined the electronic matrix elements involved and concluded that the direct mechanism to singlet fission plays an entirely negligible role in **2** and **3**, and that even the normally dominant mediated mechanism cannot contribute much, because of the way in which the two halves of the dimers are connected. The argument applies even more strongly to the covalent dimers of tetracene examined by others earlier.[17,18] Even if two-step singlet fission in our covalent dimers **2** and **3** in polar solvents does take place via the real polar intermediates observed, and triplet formation is not due to ordinary intersystem crossing, it does not compete well with loss channels. At this point, it raises interesting mechanistic issues but does not appear to offer an advantageous route to efficiency.

ASSOCIATED CONTENT

Supporting Information

Supporting Information available: synthetic procedures, triplet yield measurements, modeling of spectrotemporal data, DOSY NMR, methods of calculation, and computational results: molecular geometries (Chart S1 and Table S1), charge distribution in the charge-transfer state (Figure S1), and electronic transitions (Tables S2−S7). This material is available free of charge via the Internet at http://pubs.acs.org.

AUTHOR INFORMATION

Notes

The authors declare no competing financial interest.

ACKNOWLEDGMENTS

This material is based upon work supported by the U.S. Department of Energy, Office of Basic Energy Sciences, Division of Chemical and Biosciences, under Contract DE-AC36-08GO28308 with NREL for optical spectroscopy of dimers, DE-SC0007004 at CU-Boulder for dimer synthesis and calculations, and DE-AC02-98-CH10886 with BNL for pulsed radiolysis experiments including use of the LEAF Facility of the BNL Accelerator Center for Energy Research. Theoretical work at Northwestern University was supported by the MRSEC program and the Northwestern Materials Research Science and Engineering Center (DMR-1121262). Theory work in Prague was supported by the Institute of Organic Chemistry and Biochemistry (RVO:61388963) and the Czech Science Foundation (P208/12/G016).

REFERENCES

(1) Smith, M. B.; Michl, J. Singlet Fission. *Chem. Rev.* **2010**, *110*, 6891−6936.

(2) Nozik, A. J.; Ellingson, R. J.; Mićić, O. I.; Blackburn, J. L.; Yu, P.; Murphy, J. E.; Beard, M. C.; Rumbles, G. Unique Approaches to Solar Photon Conversion Based on Semiconductor Nanostructures and Novel Molecular Chromophores; Dynamics of Electron Relaxation, Interfacial Charge Transfer, and Carrier Multiplication. *Proceedings of the 27th DOE Solar Photochemistry Research Conference*, June 6−9, 2004, Airline Conference Center, Warrenton, VA, pp 63−66. Available online: http://science.energy.gov/~/media/bes/csgb/pdf/docs/solar_photochemistry_2004.pdf.

(3) Hanna, M.; Nozik, A. J. Solar Conversion Efficiency of Photovoltaic and Photoelectrolysis Cells with Carrier Multiplication Absorbers. *J. Appl. Phys.* **2006**, *100*, 074510/1−074510/8.

(4) Shockley, W.; Queisser, H. J. Detailed Balance Limit of Efficiency of *p*−*n* Junction Solar Cells. *J. Appl. Phys.* **1961**, *32*, 510−519.

(5) Paci, I.; Johnson, J. C.; Chen, X.; Rana, G.; Popović, D.; David, D. E.; Nozik, A. J.; Ratner, M. A.; Michl, J. Singlet Fission for Dye-Sensitized Solar Cells: Can a Suitable Sensitizer Be Found? *J. Am. Chem. Soc.* **2006**, *128*, 16546−16553.

(6) Johnson, J. C.; Nozik, A. J.; Michl, J. The Role of Chromophore Coupling in Singlet Fission. *Acc. Chem. Res.* **2013**, DOI: 10.1021/ar300193r.

(7) Burdett, J.; Müller, A. M.; Gosztola, D.; Bardeen, C. J. Excited State Dynamics in Solid and Monomeric Tetracene: The Roles of Superradiance and Exciton Fission. *J. Chem. Phys.* **2010**, *133*, 144506−144517.

(8) Lee, J.; Jadhav, P.; Baldo, M. A. High Efficiency Organic Multilayer Photodetectors Based on Singlet Exciton Fission. *Appl. Phys. Lett.* **2009**, *95*, 033301−033303.

(9) Rao, A.; Wilson, M. W. B.; Hodgkiss, J. M.; Albert-Seifried, S.; Bässler, H.; Friend, R. H. Exciton Fission and Charge Generation via Triplet Excitons in Pentacene/C_{60} Bilayers. *J. Am. Chem. Soc.* **2010**, *132*, 12698−12703.

(10) Roberts, S. T.; McAnally, R. E.; Mastron, J. N.; Webber, D. H.; Whited, M. T.; Brutchey, R. L.; Thompson, M. E.; Bradforth, S. E. Efficient Singlet Fission Found in a Disordered Acene Film. *J. Am. Chem. Soc.* **2012**, *134*, 6388−6400.

(11) Ramanan, C.; Smeigh, A. L.; Anthony, J. E.; Marks, T. J.; Wasielewski, M. R. Competition between Singlet Fission and Charge Separation in Solution-Processed Blend Films of 6,13-Bis(triisopropylsilylethynyl)pentacene with Sterically-Encumbered Perylene-3,4:9,10-bis(dicarboximide)s. *J. Am. Chem. Soc.* **2012**, *134*, 386−397.

(12) Chen, Y.; Lee, B.; Fu, D.; Podzorov, V. The Origin of a 650 nm Photoluminescence Band in Rubrene. *Adv. Mater.* **2011**, *23*, 5370−5375.

(13) Ryasnyanskiy, A.; Biaggio, I. Triplet Exciton Dynamics in Rubrene Single Crystals. *Phys. Rev. B: Condens. Matter Mater. Phys.* **2011**, *84*, 193203−193206.

(14) Wang, C.; Tauber, M. J. High-Yield Singlet Fission in a Zeaxanthin Aggregate Observed by Picosecond Resonance Raman Spectroscopy. *J. Am. Chem. Soc.* **2010**, *132*, 13988−13991.

(15) Johnson, J. C.; Nozik, A. J.; Michl, J. High Triplet Yield from Singlet Fission in a Thin Film of 1,3-Diphenylisobenzofuran. *J. Am. Chem. Soc.* **2010**, *132*, 16302−16303.

(16) Schwerin, A. F.; Johnson, J. C.; Smith, M. B.; Sreearunothai, P.; Popović, D.; Černý, J.; Havlas, Z.; Paci, I.; Akdag, A.; MacLeod, M. K.; et al. Toward Designed Singlet Fission: Electronic States and

Photophysics of 1,3-Diphenylisobenzofuran. *J. Phys. Chem. A* **2010**, *114*, 1457−1473.
(17) Müller, A. M.; Avlasevich, Y. A.; Müllen, K.; Bardeen, C. J. Evidence for Exciton Fission and Fusion in a Covalently Linked Tetracene Dimer. *Chem. Phys. Lett.* **2006**, *421*, 518−522.
(18) Müller, A. M.; Avlasevich, Y. A.; Schuller, W. W.; Mullen, K.; Bardeen, C. J. Exciton Fission and Fusion in Bis(tetracene) Molecules with Different Covalent Linker Structures. *J. Am. Chem. Soc.* **2006**, *129*, 14240−14250.
(19) Michl, J.; Nozik, A. J.; Chen, X.; Johnson, J. C.; Rana, G.; Akdag, A.; Schwerin, A. F. Toward Singlet Fission for Excitonic Solar Cells. In *Organic Photovoltaics VIII*; Kafafi, Z. H., Lane, P. A., Eds.; Proceedings of SPIE; SPIE: Bellingham, WA, 2007; Vol. *6656*, p 66560E1.
(20) Würthner, F.; Kaiser, T. E.; Saha-Möller, C. R. J-Aggregates: From Serendipitous Discovery to Supramolecular Engineering of Functional Dye Materials. *Angew. Chem., Int. Ed.* **2011**, *50*, 3376−3410.
(21) Furlan, A.; Riley, M. J.; Leutwyler, S. The Jahn−Teller Effect in Triptycene. *J. Chem. Phys.* **1992**, *96*, 7306−7320.
(22) Greyson, E. C.; Stepp, B. R.; Chen, X.; Schwerin, A. F.; Paci, I.; Smith, M. B.; Akdag, A.; Johnson, J. C.; Nozik, A. J.; Michl, J.; et al. Singlet Exciton Fission for Solar Cell Applications: Energy Aspects of Interchromophore Coupling. *J. Phys. Chem. B* **2010**, *114*, 14223−14232.
(23) Chan, W. L.; Ligges, M.; Jailaubekov, A.; Kaake, L.; Miaja-Avila, L.; Zhu, X. Y. Observing the Multiexciton State in Singlet Fission and Ensuing Ultrafast Multielectron Transfer. *Science* **2011**, *334*, 1541−1545.
(24) Greyson, E. C.; Vura-Weis, J.; Michl, J.; Ratner, M. A. Maximizing Singlet Fission in Organic Dimers: Theoretical Investigation of Triplet Yield in the Regime of Localized Excitation and Fast Coherent Electron Transfer. *J. Phys. Chem. B* **2010**, *114*, 14168−14177.
(25) Teichen, P. E.; Eaves, J. D. A Microscopic Model of Singlet Fission. *J. Phys. Chem. B* **2012**, *116*, 11473−11481.
(26) Stevens, B.; Marsh, K. L; Baltrop, J. A. Photoperoxidation of Unsaturated Organic Molecules. 21. Sensitizer Yields of O_2 $^1\Delta_g$. *J. Phys. Chem.* **1981**, *85*, 3079−3082.
(27) Johnson, J. C.; Gerth, K. A.; Song, Q.; Murphy, J. E.; Scholes, G. D.; Nozik, A. J. Ultrafast Exciton Fine Structure Relaxation Dynamics in Lead Chalcogenide Nanocrystals. *Nano Lett.* **2008**, *8*, 1374−1381.
(28) http://www.wavemetrics.com/products/igorpro/igorpro.htm.
(29) Stokkum, I. H. M.; Larsen, D. S.; van Grondelle, R. Global and Target Analysis of Time-Resolved Spectra. *Biochim. Biophys. Acta* **2004**, *1657*, 82−104.
(30) Hauser, C. R.; Tetenbaum, M. T.; Hoffenberg, D. S. Condensations Involving the Metalation of the 3-Position of 3-Phenylphthalide by Means of Alkali Amides. Carbonation of Phthalide. *J. Org. Chem.* **1958**, *23*, 861−865.
(31) Newman, M. S. Evidence Favoring a Two-Step Mechanism for the Diels−Alder Reaction. *J. Org. Chem.* **1961**, *26*, 2630−2633.
(32) Streitwieser, A.; Vorpagel, E. R.; Chen, C.-C. Carbon Acidity. 66. Equilibrium Ion Pair Acidities of Substituted Diphenylmethanes in Cyclohexylamine. *J. Am. Chem. Soc.* **1985**, *107*, 6970−6975.
(33) Helms, A.; Heiler, D.; McLendon, D. Electron Transfer in Bis-porphyrin Donor−Acceptor Compounds with Polyphenylene Spacers Shows a Weak Distance Dependence. *J. Am. Chem. Soc.* **1992**, *114*, 6227−6238.
(34) Dodge, J. A.; Bain, J. D.; Chamberlin, A. R. Regioselective Synthesis of Substituted Rubrenes. *J. Org. Chem.* **1990**, *55*, 4190−4198.
(35) Jacq, J.; Tsekhanovich, S.; Orio, M.; Einhorn, C.; Einhorn, J.; Bessières, B.; Chauvin, J.; Jouvenot, D.; Loiseau, F. Structure and Dynamics of the Excited States of 1,3-diarylisobenzofurans: An Experimental and Theoretical Study. *Photochem. Photobiol.* **2012**, *88*, 633−638.
(36) Grabowski, Z. R.; Rotkiewicz, K.; Rettig, W. Structural Changes Accompanying Intramolecular Electron Transfer: Focus on Twisted Intramolecular Charge-Transfer States and Structures. *Chem. Rev.* **2003**, *103*, 3899−4032.
(37) Dobkowski, J.; Wójcik, J.; Koźmiński, W.; Kołos, R.; Waluk, J.; Michl, J. An Experimental Test of C−N Bond Twisting in the TICT State: Syn−Anti Photoisomerization in 2-(*N*-Methyl-*N*-isopropylamino)-5-cyanopyridine. *J. Am. Chem. Soc.* **2002**, *124*, 2406−2407.
(38) Dreuw, A.; Weisman, J. L.; Head-Gordon, M. Long-Range Charge-Transfer Excited States in Time-Dependent Density Functional Theory Require Non-local Exchange. *J. Chem. Phys.* **2003**, *119*, 2943−2946.
(39) Gritsenko, O.; Baerends, E. J. Asymptotic Correction of the Exchange-Correlation Kernel of Time-Dependent Density Functional Theory for Long-Range Charge-Transfer Excitations. *J. Chem. Phys.* **2004**, *121*, 655−670.
(40) Autschbach, J. Charge-Transfer Excitations and Time-Dependent Density Functional Theory: Problems and Some Proposed Solutions. *ChemPhysChem* **2009**, *10*, 1757−1760.
(41) Figure 66 and associated text on p. 3954 of ref 36.
(42) Smith, M. B.; Michl, J. Recent Advances in Singlet Fission. *Annu. Rev. Phys. Chem.* **2013**, *64*, 361−386.
(43) Bonačić-Koutecký, V.; Michl, J.; Köhler, J. Prediction of Structural and Environmental Effects on the S_1−S_0 Energy Gap and Jump Probability in Double-Bond *cis*−*trans* Photoisomerization. A General Rule. *Chem. Phys. Lett.* **1984**, *104*, 440−443.
(44) Schneider, F.; Lippert, E. Elektronenspektren und Elektronenstruktur von 9,9′-Dianthryl. *Ber. Bunsenges. Phys. Chem.* **1968**, *72*, 1155−1160.
(45) Kang, T. J.; Kahlow, M. A.; Giser, D.; Swallen, S.; Nagarajan, V.; Jarzeba, W.; Barbara, P. F. Dynamic Solvent Effects in the Electron-Transfer Kinetics of S_1 Bianthryls. *J. Phys. Chem.* **1988**, *92*, 6800−6807.
(46) Elich, K.; Kitazawa, M.; Okada, T.; Wortmann, R. Effect of S_1 Torsional Dynamics on the Time-Resolved Fluorescence Spectra of 9,9′-Bianthryl in Solution. *J. Phys. Chem. A* **1997**, *101*, 2010−2015.
(47) Mac, M.; Kwiatkowski, P.; Pischel, U. Temperature Dependence of Bianthryl Dual Fluorescence. *Chem. Phys. Lett.* **2002**, *357*, 440−449.
(48) Dance, Z. E. X.; Mickley, S. M.; Wilson, T. M.; Ricks, A. B.; Scott, A. M.; Ratner, M. A.; Wasielewski, M. R. Intersystem Crossing Mediated by Photoinduced Intramolecular Charge Transfer: Julolidine−Anthracene Molecules with Perpendicular p Systems. *J. Phys. Chem. A* **2008**, *112*, 4194−4201.